High-Strength Steels

by H. K. D. H. Bhadeshia

"Future Developments of Metals and Ceramics"

eds J. A. Charles, G. W. Greenwood and G. C. Smith

Institute of Materials, London (1992) pp. 25--74

High-Strength Steels

H. K. D. H. Bhadeshia

Lecturer, Department of Materials Science and Metallurgy
The University of Cambridge

Abstract
Systematic alloy design combined with innovative technology has led to the successful exploitation of new ultra high strength steels. The physical metallurgy of some of the latest of these strong steels is summarised, with a view to reflecting the exciting state of both the basic research and the commercial enterprise behind the developments.

1. Introduction

The awesome technology apparent in modern steel manufacturing facilities is impressive, but much more so is the fundamental versatility of iron, which has its origins in the electronic, atomic and crystal structure of elemental iron, as first appreciated in the classic work of Zener.[1] There are three allotropic forms of iron, α (ferrite, body centered cubic), γ (austenite, cubic close packed) and ε (hexagonal close packed). The ε iron is the most dense allotrope and consequently the most stable at high pressures. α iron undergoes a paramagnetic to ferromagnetic transition on cooling below about 1042 K, the effects of which were at one time incorrectly attributed to the presence of a further allotrope, β iron.

γ iron is considered to exist in two electronic states separated by a narrow energy gap, the state stable at high temperatures being ferromagnetic (Curie temperature 1800 K) with a magnetic moment of about 2 Bohr magnetons per atom, similar to that of α iron.[2,3] At low temperatures, γ iron is in the lower energy antiferromagnetic state, with a magnetic moment of 0.56–0.70 Bhor magnetons per atom and a Néel temperature below 80 K.[4–6] The two states of γ iron have different molar volumes. On the grounds that the Debye temperatures and electronic specific heat coefficients of ferrite and austenite are equal, they should also have the same thermal expansion coefficients. However, because the densities of the two forms of austenite differ significantly, and because the relative proportions of atoms in the two forms change with temperature, the apparent expansion coefficient of austenite as a whole is much larger than that of ferrite.

All this explains the peculiar behaviour of iron at ambient pressure, i.e., that α is stable at low temperatures, γ at intermediate temperatures and α again at temperatures close to the melting point. Ferrite is stable relative to austenite at low temperatures, but the two-spin state electronic structure of austenite gives it an extra entropy which stabilises it above 1185 K. The reversion to ferrite above 1667 K results from its magnetic entropy which builds up rapidly above the Curie temperature and eventually overcomes the two-spin entropy of austenite.

These descriptions help rationalise the allotropes of iron, but the transformations between the allotropes can occur by many mechanisms, giving rise to a variety of microstructures. The addition of carbon introduces further variants of microstructure, and of substitutional solutes an incredibly rich variety of microstructures. This versatility, and the demonstrated ability of the steel industry to exploit it, is responsible for the amazing success of steels.[7] Thus, any paper such as this necessarily addresses only a miniscule proportion of the research and developments in the technology and science of steels. The aim here is to present an outline of the physical metallurgy of new high strength steels and iron alloys.

2. The Highest Strength of All

Marageing steels are essentially martensitic alloys containing only traces of carbon but unusually large concentrations of nickel, cobalt and molybdenum. They were invented at the INCO laboratories in the USA and a conscious decision was taken to market the alloys as steels (rather than as ferrous alloys) in spite of the very low carbon concentrations.[8] It is this lack of carbon which makes them incredibly tough. The strength is derived by aging the martensite at temperatures where substitutional solutes are mobile, in order to allow the precipitation of strengthening intermetallic compounds such as Ni_3Mo. The intermetallic compounds are not themselves brittle and are coherent with the matrix, so that they do not nucleate cracks or voids. Hornbogen,[9] in 1987, published an assessment of steels with yield strengths exceeding 3 GPa. In that assessment, he addressed mainly marageing steels (Fig. 1). He concluded that a value of 3.5 GPa seems to represent an upper limit for the yield strength of steels. As will be seen later, this prediction was soon afterwards proved incorrect, with commercial steels having strength levels in excess of 5 GPa.

It is in fact necessary to go back to the fundamentals of metallurgy to set the upper limit to the strength of a material. The ideal slip resistance of a metal is about $G/30$, where G is the elastic modulus in shear. It is well established that this impressive level of strength can be achieved as the crystal becomes smaller in size.[10] In fact, crystals in the form of whiskers can be so strong that *elastic* strains of the order of a few per cent can easily

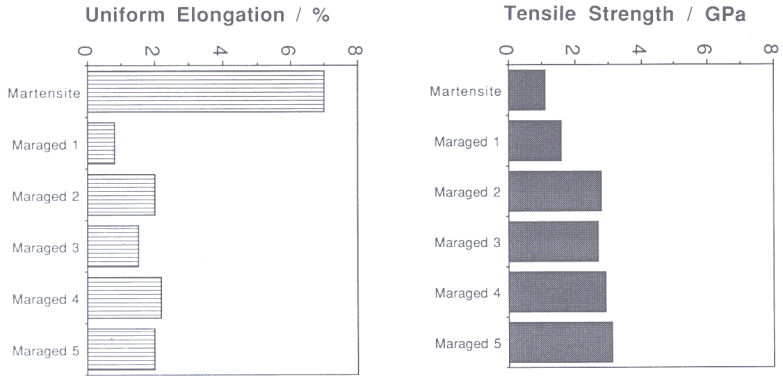

Fig. 1. Typical values of the mechanical properties of a variety of heat treated or thermomechanically processed marageing steels (after Hornbogen).[9] *The 'martensite' represents as-quenched marageing steel, 'maraged 1' represents quenched and maraged steel, and the others are all thermomechanically processed in a variety of ways.*

be achieved, with nonlinear elastic phenomena manifesting at the larger strains (Fig. 2). It is interesting to note that the strain energy stored in a unit of volume of the iron whisker crystal characterised in Fig. 2, at its breaking strength, is approximately 20% of that found in the explosive used for the manufacture of munitions (typically 3×10^9J m^{-3}). Micrometer sized, whisker shaped single crystals are strong because they tend either to be free of dislocations, or because each crystal might contain just a single sessile dislocation along the long dimension. In the absence of glissile dislocations, the strength is determined by the critical resolved shear stress needed to accomplish the cooperative glide of entire planes of

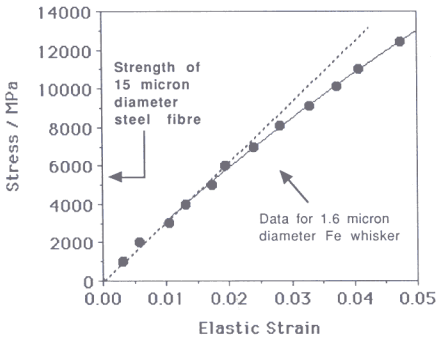

Fig. 2. Stress versus elastic strain curve for a single-crystal iron whisker.[10] *The dashed line is straight. The fibre characteristics will be discussed later in the text.*

atoms over each other, or by the stress necessary to pull the layers of atoms apart (ideal cleavage). Dislocations reduce the strength by accomplishing the glide in a piecemeal fashion, with gross distortions being localised in the close proximity of the dislocation core.

Thus, strength can easily be achieved, but its utilisation may require a consideration of other factors such as toughness, ease of manufacture, cost, etc. There do not appear to be any major applications of iron or other metallic whiskers to date, perhaps because they have been forgotten by modern materials scientists. It is conceivable that the situation could change if the whiskers were to be produced cheaply and on a large scale.

Many applications require continuous fibres. In the case of steels, such fibres are made by drawing. The process relies heavily on the fact that the stresses involved in the drawing operation do not lead to necking instabilities, so that very large strains can be achieved without fracture.[11] Drawing can be used on an industrial scale to fabricate wires with diameters as small as a few micrometers. *Encyclopaedia Britannica*[12] lists the fact that 1 g of gold has been drawn into a very fine fibre of length about 3 km. Continuous fibres of steel are now available commercially at diameters less than 10μm so that a gram of steel can now be drawn to a length in excess of 3 km!

For most commercial purposes, the steel fibres are wound together to form multifilamentary strands. Repetition of this in a self-similar way can enable the production of tenacious wires and ropes with collective diameters sometimes exceeding a metre. The main property requirements include tensile strength, ductility, wear resistance, bendability and resistance to stress relaxation.

Conventional steel wires usually have a eutectoid composition and have relied on a pearlitic microstructure for strength. The pearlite is produced in an unusually refined form by forcing the transformation of austenite to relatively low temperatures, using the *patenting* process. To achieve the necessary undercooling of the austenite prior to its transformation, the hot rod or wire of steel is cooled rapidly in air, or in some molten fluid such as lead or salt. The resulting fine pearlite is necessary to facilitate the large reductions in diameter during drawing, reductions which are essential to reach the required strength levels.[13]

The patenting process has achieved a large degree of success for many decades, and steel wires and ropes with tensile strengths around 2–3 GPa are widely used, for example in the construction of long-span suspension bridges designed to last for 25–50 years in service. In spite of the fact that the wire technology is well established, it would be foolish to suggest that there are no major developments to be expected for pearlitic wires. One interesting recent innovation in pearlitic wires is related to the fact that an increase in the carbon concentration beyond the eutectoid composition

can in fact lead to a deterioration in the mechanical properties. The precipitation of proeutectoid cementite at the austenite grain surfaces leads to embrittlement. The problem has been resolved elegantly by shifting the eutectoid composition to larger carbon concentrations using cobalt as an alloying element.[14] Cobalt is known to lessen the hardenability,[15,16] i.e. to increase the stability, of ferrite relative to austenite. It consequently modifies the phase diagram in a manner which can be exploited for the development of high-tensile wires with larger volume fractions of fine cementite as a constituent of pearlite, rather than as more brittle proeutectoid cementite.

3. Scifer

A remarkable, gigantic increase in strength (from 3 → 5 GPa) has just been achieved for steel wire with a microstructure entirely different from that of pearlite.[17] The invention brings renewed confidence to the expression 'strong as steel'. The wire, which is made by drawing, has the trade name Scifer. The product results from dedicated long term research on wire technology, and the name is a derivative of 'scientific iron'. There is nothing unusual about the chemistry of the steel involved (Fe–0.2C–0.8Si–1.Mn wt%), apart from the fact that the purity has to be consistent with the fact that the final fibre diameter is sometimes expected to be less than 10 μm. The inclusion content must therefore be kept at a minimum. The carbon concentration is much smaller than in pearlitic wires, and the silicon concentration is somewhat larger. Although the wire is drawn as for conventional piano wire, the heat treatment is radically different from that involved in the patenting process (Fig. 3).

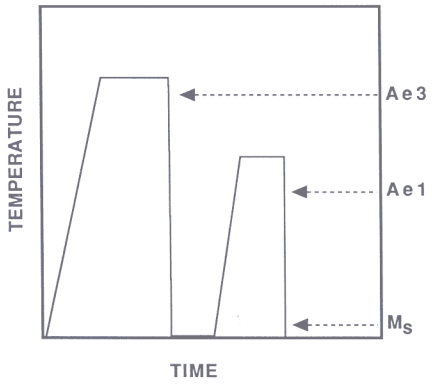

Fig. 3. Schematic illustration of the heat treatment used in the production of Scifer.

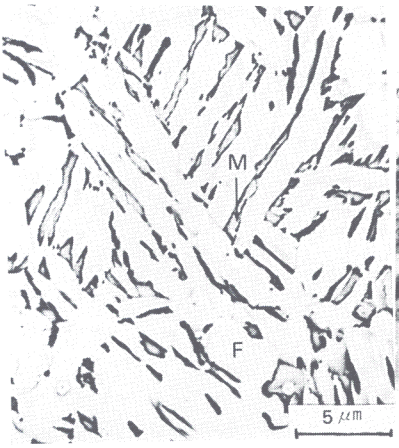

(a)

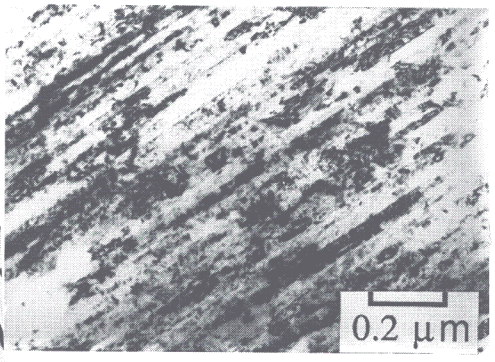

(c)

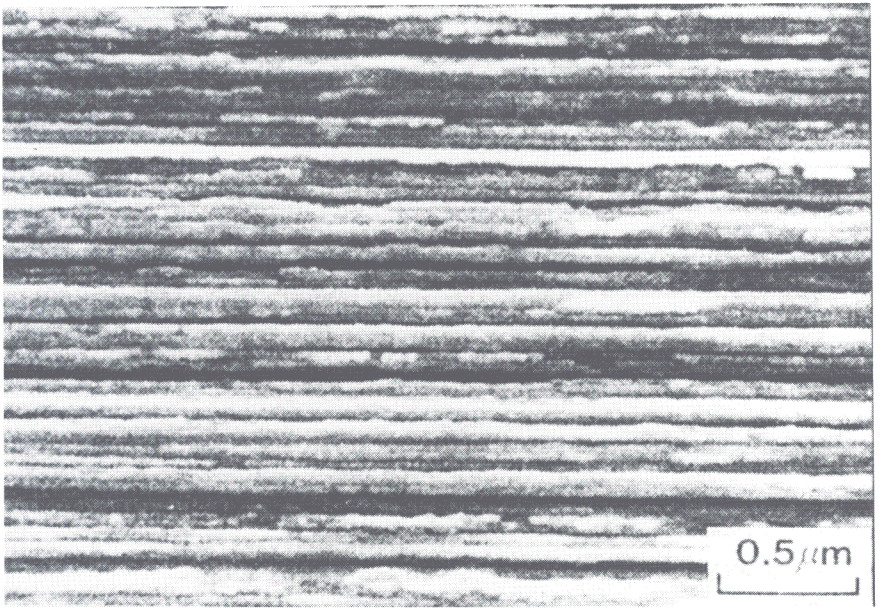

(b)

Fig. 4. (a) The microstructure of Scifer after heat treatment but prior to drawing. F refers to ferrite regions formed by the tempering of martensite during intercritical annealing, and M to areas containing martensite and retained austenite. (b) Scanning electron micrograph of the same sample after a true strain of 8.85 without intermediate annealing. The initial and final diameters of the wire are 2.5 mm and 30 micrometers respectively. (c) Transmission electron micrograph of the drawn wire.[17]

Rods of diameter 10 mm are first quenched to martensite, and then intercritically annealed in the ($\alpha + \gamma$) phase field. This induces the growth of a small quantity of austenite in the form of layers between the packets of the original martensite. The latter tempers during the intercritical anneal, and on quenching to ambient temperature the layers of austenite soon decompose into regions of high-carbon martensite and with some retained austenite (Fig. 4). The light areas in Fig. 4a are the regions of martensite which are tempered during the intercritical anneal; they probably do not contain any carbides, since the carbon is expected to migrate into the newly formed austenite. Each of these tempered martensite regions in fact contains tiny plates of martensite of mean width approximately 0.2 μm. Thus, an ultrafine starting microstructure is attained by exploiting the mechanism of martensitic transformation, since the strain energy associated with the invariant-plane strain shape deformation accompanying the growth of martensite, is minimised by the adoption of a thin plate shape. Note that the effective grain size, i.e. the mean slip distance within the plate of martensite, is almost the same as the plate thickness rather than the length, since the chances of slip in an orientation parallel to the plate habit are very small indeed.[18,19]

Transmission electron microscopy (TEM) (Fig. 4c) suggests that the microstructure of the drawn fibre in its final condition consists of a dislocation cell structure which is slightly elongated along the drawing direction. The cell size along the wire diameter is not known and their size is generally unclear from the transmission micrographs. A typical dislocation cell structure would contain dislocations localised at the cell walls, and relatively clean cell interiors. It has not yet been possible to distinguish clearly the martensitic and tempered martensitic regions in the drawn wire microstructures.

A better understanding of the microstructure is needed to explain the properties of Scifer, with a clarity beyond that revealed by transmission electron microscopy, where the confused contrast due to the strain fields of the irregular deformation structure masks important features. The atomic resolution technique of field ion microscopy (FIM) is an ideal tool for this purpose; the dislocation cell structure can be revealed by the fact that the distribution of strain energy in the proximity of a low misorientation boundary leads to preferential evaporation of material, and hence contrast in the image.[20]

Figure 5 shows FIM images of as-received Scifer in the cold drawn condition. They clearly reveal the ultrafine dislocation cell structure, the cell size in a direction normal to the drawing direction being approximately 10–15 nm. The small crystallographic misorientaions across the cell boundaries are revealed by the approximate continuity of the rings of imaged atoms across the cell walls (Fig. 5b).

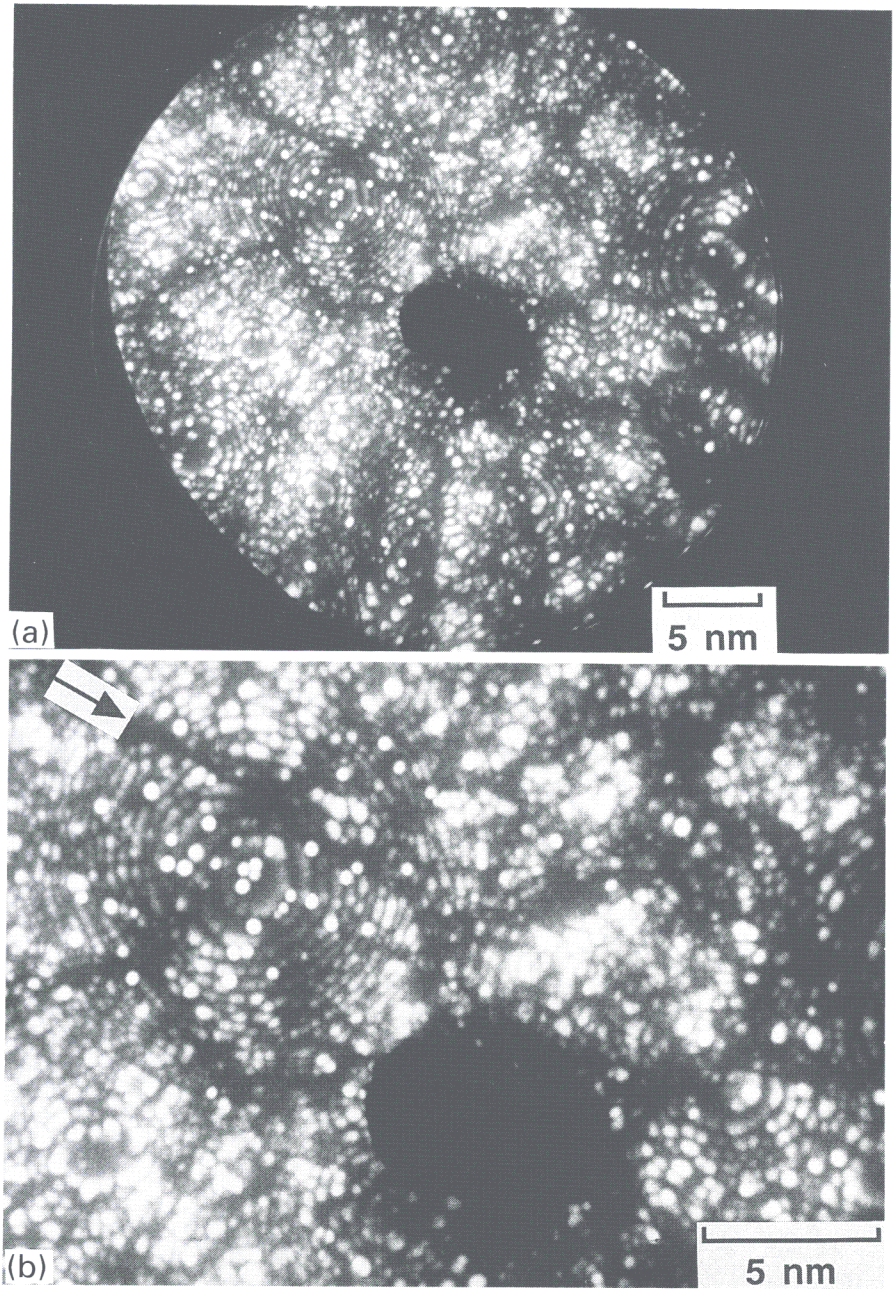

Fig. 5. Field ion images of as-received Scifer, using neon as the imaging gas and with a sample temperature of 22 K (a) Dislocation cell structure. (b) Continuity of rings of imaged atoms across the cell walls.

Table 1 Contributions to the strength (MPa) of Scifer at ambient temperature

σ_{Fe}	217
σ_{Mn}	63
σ_{Si}	83
σ_{C}	800
σ_{Cell}	3300–5000
Total (dissolved C)	4463–6163
Total (precipitated C)	3663–5363

4.1 The Strength of Scifer

According to a popular model for large grained microstructures, macroscopic yielding is determined by the spread of deformation across the grain boundaries, as the stress concentration built up due to dislocation pile-ups within a given grain initiates dislocation sources in the adjacent grain. An analysis of such a process gives the classical Hall–Petch relationship in which the yield stress depends on the inverse square root of grain size. The problem of general yield is rather different as the grain size reduces to below about 1 μm, because it is no longer the initiation of sources in an adjacent grain that determines yield. Instead, it is the stress to operate a source within a grain that is the critical event in triggering macroscopic yielding.

Langford and Cohen[21,22] have treated the problem of strengthening due to the fine cell structures formed in drawn wires. They considered the energy required to spread and expand dislocation loops across the glide planes of the cells, during the deformation of the cells along their long directions. The strength σ was found to depend on the inverse of the cell size:

$$\sigma \approx \sigma_O + 2.5Gb(\bar{d})^{-1} \quad (1)$$

where $\bar{d} \approx 10$–15 nm is the cell size normal to the drawing direction, $b \approx 0.25$ nm is the magnitude of the Burgers vector of the slip dislocation, $G \approx 80$ GPa and σ_O is the friction stress. Thus, the strengthening due to the cell size (i.e. σ_{Cell}) can easily be calculated to be approximately 5000–3300 MPa (for $d \approx 5$–15 nm). The cell structure clearly is the major contribution to the total strength of the wire. The term σ_O can be factorised as follows:

$$\sigma_O \approx \sigma_{Fe} + \sum_i \sigma_i \quad (2)$$

where σ_{Fe} is the strength of pure annealed iron at ambient temperature, and σ_i are the contributions from solid solution strengthening. Using published data,[23–25] it is possible to arrive at the strength contributions listed in Table 1. Thus the total yield strength is estimated to be about 4.5–

6.2 GPa, if all the carbon is assumed to be in solid solution, and 3.7–5.4 GPa if the carbon is precipitated and therefore assumed to contribute little to the overall strength. Clearly, the sum of the contributions listed in Table 1 compare rather well with the available data on the *tensile* strength of Scifer at 4–5.3 GPa (Fig. 6).

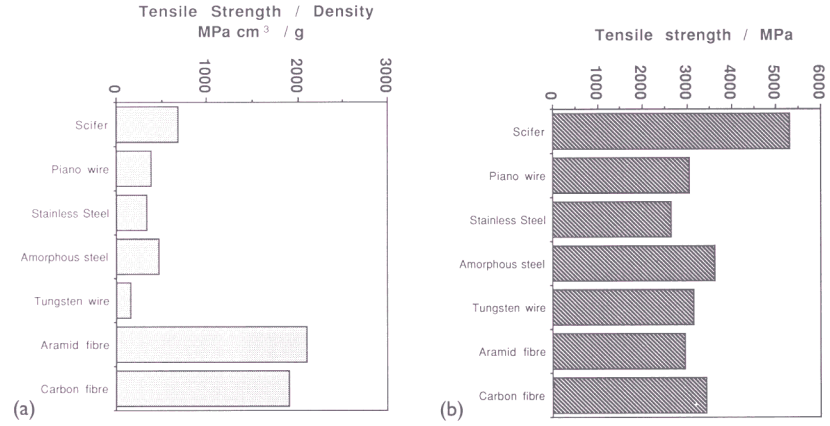

Fig. 6. A comparison of the proportion of a variety of materials used in the manufacture of fibres or ropes. The experimental data on Scifer are from Ref. 17. (a) strength; (b) specific strength.

4.2 *The Role of Carbon*

The function of carbon in Scifer is interesting and requires some further investigation and comment. The intercritical annealing heat treatment (followed by quenching to ambient temperature) should give a microstructure of high carbon martensite (C > 0.2 wt%), its associated small quantity of retained austenite, and ferrite. There is also the possibility of some minute cementite particles due to any autotempering of the martensite, although TEM has not revealed it. This is the microstructure before any deformation.

Atom probe experiments have been carried out on a field ion microscope to understand better the distribution of carbon in the high strength steel wire after the severe drawing deformation.[26] Time-of-flight mass spectroscopy can easily reveal the concentration in solid solution. Figure 7 shows data obtained during depth profiling as the as-received sample was field evaporated. The data are collected on an atom by atom basis, but to visualise the concentration, they are presented as the concentrations of carbon in each successive block of 100 or 1000 atoms. Note that the presence of a carbide would lead to a carbon concentration of around 25 at %. It is therefore clear that the composition profiles represent carbon in solid solution, the average carbon concentration of some 111378 ions

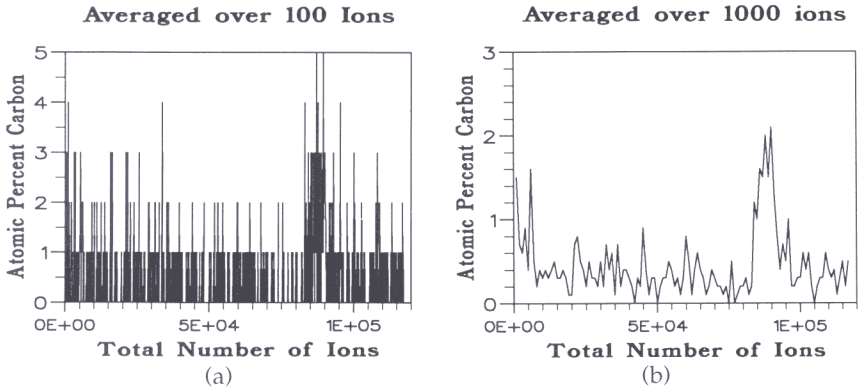

Fig. 7. Carbon concentration of the ferrite in as-received Scifer wire (a) Averaged over each successive 100 ion block (b) Averaged over each successive 1000 ion block.

collected being 0.5 ± 0.2 at % (i.e. 0.11 wt%). Thus, a great excess of carbon is present in solid solution in the ferrite, amounting to about half the total carbon concentration of the alloy (0.2 wt%).

The combined results from a large number of experiments are presented in Fig. 8. The very large but extremely narrow carbon spike seen in Fig. 8a was observed while probing into a cell boundary, and could indicate either the presence of extremely small carbides (100 atoms at most) or more likely, the segregation of carbon in regions of large dislocation density. An additional experiment was conducted by annealing the deformed wire at 400°C for 90 mins. Field ion images confirmed that this had no observable effect on the dislocation structure, although the appearance of several relatively broad carbon spikes during depth profiling indicated that the annealing treatment was inducing the precipitation of some very fine carbides (Fig. 8b).

The starting microstructure prior to deformation contained regions of martensite formed during intercritical annealing, which are expected to contain carbon concentrations far in excess of the average level of 0.2 wt%. Instead, the results show that there is a relatively uniform carbon concentration in the matrix at a concentration of about 0.1 wt%, with no signs of carbide particles. They confirm directly that there is a large excess of carbon trapped in solid solution in the ferrite. It appears that the extreme degree of deformation required to produce the fibre has led to a *mechanical homogenisation* of the starting microstructure.*

* This phenomenon will be discussed again in the section that follows on 'mechanical alloying'.

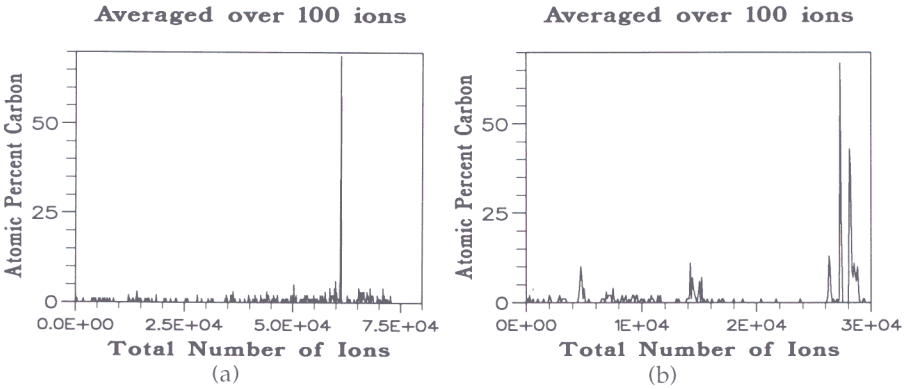

Fig. 8. Carbon concentration profiles (a) as-received wire (b) after annealing at 400°C for 90 minutes.

It is interesting to note that similar mechanical homogenisation effects have been reported when mixed microstructures of ferrite and cementite are heavily deformed. Whilst the solubility of carbon in ferrite which is in equilibrium with cementite is very small indeed, large deformations are well known to force the dissolution of cementite, at temperatures below that of which austenite might form first. This is commonly assumed to happen in the region of intense deformation during the ballistic penetration of steel. The formation of the so-called 'white layers' on pearlitic rail steels subjected to severe deformation is another example of this phenomenon. The white layers are believed to form without any growth of austenite, but the carbon nevertheless enters solid solution in the ferrite.[27] There are two mechanisms known to induce carbide dissolution in metastable microstructures. Firstly, the deformation causes a fragmentation of the cementite to a size well below its critical nucleus size, so that the cementite dissolves. Secondly, the stability of precipitates is known to be affected by the presence of dislocations, where the carbon may segregate in preference to precipitation.[28,29]

4.3 Size Sensitivity

The very high strength of a whisker crystal of iron is attributed to the absence of glissile dislocations, necessitating the coordinated slip of entire planes of atoms. Dislocations therefore weaken whisker crystals. Consequently, their strength collapses rapidly with increasing size, because the chances of finding dislocations are larger in bigger samples (Fig. 9). Scifer, on the other hand, is far less sensitive to the fibre diameter, because its strength originates from the presence of dislocations in the form of ultra-

fine cells (Fig. 9). Indeed, for the range of diameters available, the strength of Scifer is much larger than that of whiskers. It must be concluded that the observed mild size sensitivity of Scifer arises due to the presence of defects other than dislocations, for example, nonmetallic particles. In some respects this phenomenon is reminiscent of the behaviour of glass fibres, whose strength increases as the size decreases. The probability of finding defects in the fibre is reduced as the size decreases. Thus, glass fibres can be forced into relatively large curvatures, whereas in much less severe circumstances, a glass rod is expected to shatter.

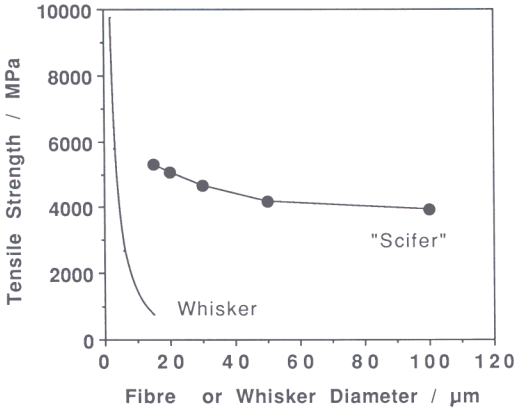

Fig. 9. A comparison of the size sensitivity of whiskers and the steel fibre Scifer. The experimental data on Scifer are from Ref. 17.

4.4 Ductility of Scifer

Scifer fails in a ductile manner during tensile testing (Fig. 10); given the incredibly fine fibre size, it is extremely unlikely that plane–strain conditions ever arise. The high purity necessary to ensure drawability leads to a small inclusion content. Thus void nucleation is relatively difficult. Any voids that do form must extend considerably before linking, thereby ensuring an increased value of elongation.

4.5 Applications of Scifer

Figure 10 shows that Scifer has remarkable ductility considering its strength, and the mode of failure in tension is found to involve considerable necking, as is clear from the reduction of area. This ductility gives the fibre a high degree of reliability, making it possible to bend and twist the fibres without failure (the fibre can in fact be tied into a tight knot). The elastic modulus (> 200 GPa) is only slightly smaller than that of carbon fibre.

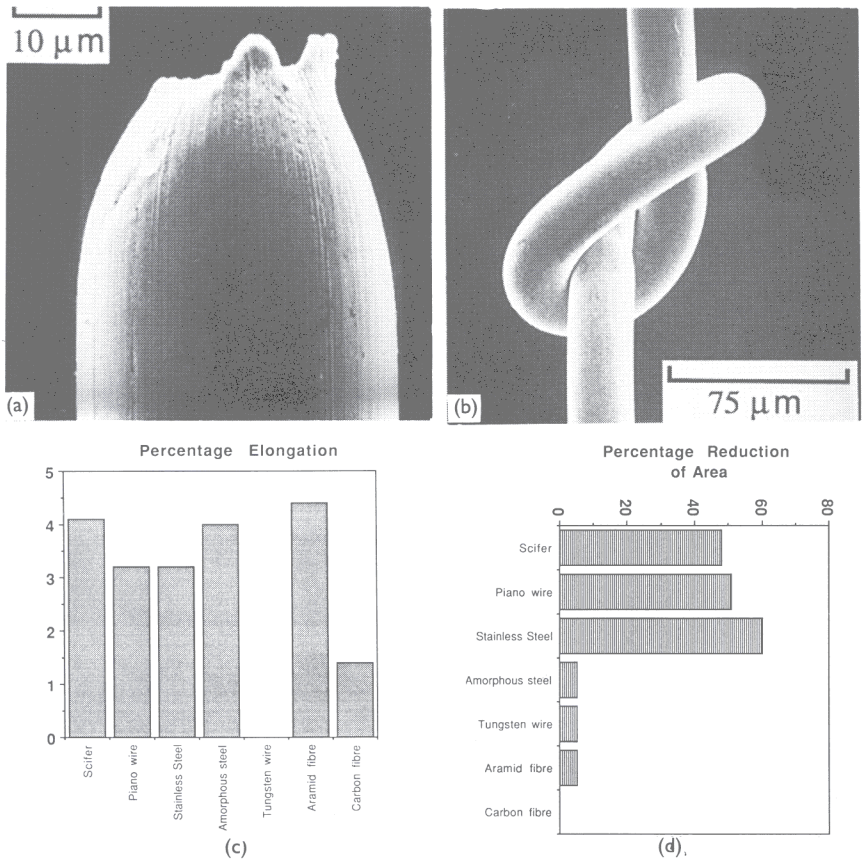

Fig. 10. (a) Scanning electron micrograph of a fractured Scifer fibre, and (b) of a fibre tied into a tight knot. Comparison of the (c) elongation and (d) reduction of area of Scifer against other commercial fibres. Data from Ref. 17.

In their filamentary form, the ultra-thin fibres are available for use in the cutting and polishing of semiconductors, ceramics and diamonds, and for the fabrication of miniature springs for microscopic machines. Large scale applications are envisaged for multifilamentary strands, as cables for aircraft and telecommunications, fibre reinforcement for rubbers, plastics and metals, and in their nickel plated and resin coated form, as fishing lines.

5. Mechanically Alloyed Steels

5.1 On Solid Solutions and Mechanical Mixtures

The concept of a *solid solution* is familiar to most metallurgists and engineers, so much so that it is probably taken for granted. There is now a

new alloy fabrication route invented by Benjamin,[30] the discussion of which warrants first a reminder of the difference between a solid solution and a physical mixture of fine elemental powders.

If interfacial energy is neglected, then the molar Gibbs free energy of a mechanical mixture of two elemental substances (*A* and *B*) is given by a weighted average of the molar free energies of the pure components:

$$G_M = \chi_A G^\circ_A + (1 - \chi_A) G^\circ_B \tag{3}$$

where χ_A is the mole fraction of substance *A*. This is essentially a rule of mixtures, with atoms of species *A* being largely unaware of the presence of the *B* atoms. The sample is physically divided into macroscopic regions containing either just the *A* or the *B* atoms. Thus, the total number of patterns that can be generated, by swapping atomic positions (i.e. the configurations) within each component of the mixture, is unaltered by making a mechanical mixture.

A solid solution on the other hand, is an *intimate* mixture on an atomic scale, in such a way that the system recognises the presence of the two different kinds of atoms. There is always a change in configurational entropy, the term in thermodynamic theory which accounts for the many more atomic configurations that become possible when a solid solution forms. There may also be a change in the binding energies, since some of the original atomic bonds are broken while new ones are formed. This manifests itself as a molar enthalpy of mixing (H_M). The free energy of a solid solution is therefore given by:

$$G_M = \chi_A G^\circ_A + (1 - \chi_A) G^\circ_B + \chi_A (1 - \chi_A) H_M - T S_M \tag{4}$$

where *T* is the absolute temperature, $S_M = -R[\chi_A \ln\{1 - \chi_A\} + (1 - \chi_A) \ln\{\chi_A\}]$ is the molar entropy of mixing, and *R* is the universal gas constant. For an ideal solution (one which is random), the entropy of mixing is simply the change in the configurational entropy of mixing, and this may be used as an approximation even when the solution is not ideal. This then is the fundamental difference between a mechanical mixture and a solid solution.

Figure 11 illustrates these concepts schematically. The straight line joining the points G°_A and G°_B represents the free energy of mechanical mixtures, whereas the curves the free energies of two different kinds of solid solutions (marked *M* and *N* on Fig. 11a). It is a fundamental principle of such diagrams that the curves representing solid solutions must end tangentially at the vertical axes, since there is a large change in configurational entropy as soon as even a single foreign atom is added to the pure component.

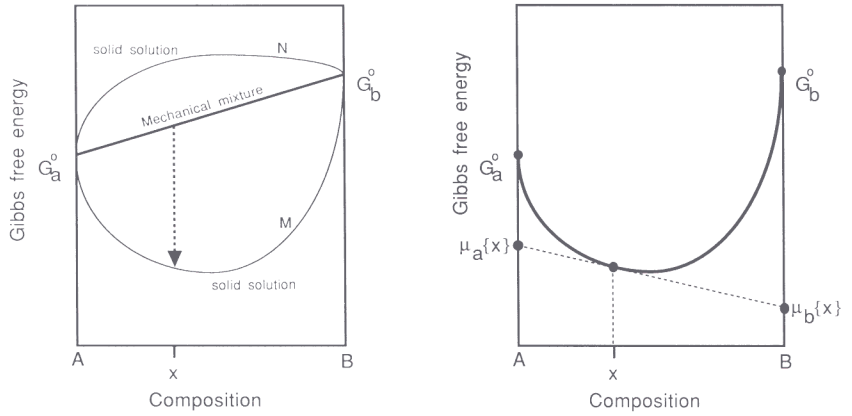

Fig. 11. (a) Free energy curves for solid solutions and a straight line representing a mechanical mixture. (b) Illustration of the concept of a chemical potential.

To discuss the two kinds of solid solutions illustrated in Fig. 11, it is necessary to understand the concept of a chemical potential. The chemical potentials (μ) of the elements are defined by the equation:

$$G_M = \chi_A \mu_A + (1 - \chi_A)\mu_B. \tag{5}$$

It should be evident from this equation, that the physical meaning of the chemical potential is simply that μ_A represents the average free energy of a mole of *A* atoms *in a solution* of composition χ_A. On the diagram illustrated in Fig. 11b, the chemical potentials of *A* and *B* in any solution of composition χ is given by drawing a tangent to the free curve, and noting the intercepts on the vertical axes.

The arrow in Fig. 11a illustrates the case where there is a net reduction of free energy on converting the mechanical mixture into a solid solution (curve M). It represents an instant where the *A* and *B* atoms like each other and prefer to be in solution; the chemical potentials of both kinds of atoms are reduced on forming the solution. The other kind of solution illustrated by the curve N above the mechanical mixture line (Fig. 11a) represents the case where the *A* and *B* atoms prefer not to mix, so that there is a net increase in the free energy on forming a solution from a mechanical mixture. A tangent drawn to that free energy curve for *any* composition would indicate that the chemical potentials of both species are increased above the free energies of the pure components (G°_A and G°_B). When the chemical potential of an element is increased on entering

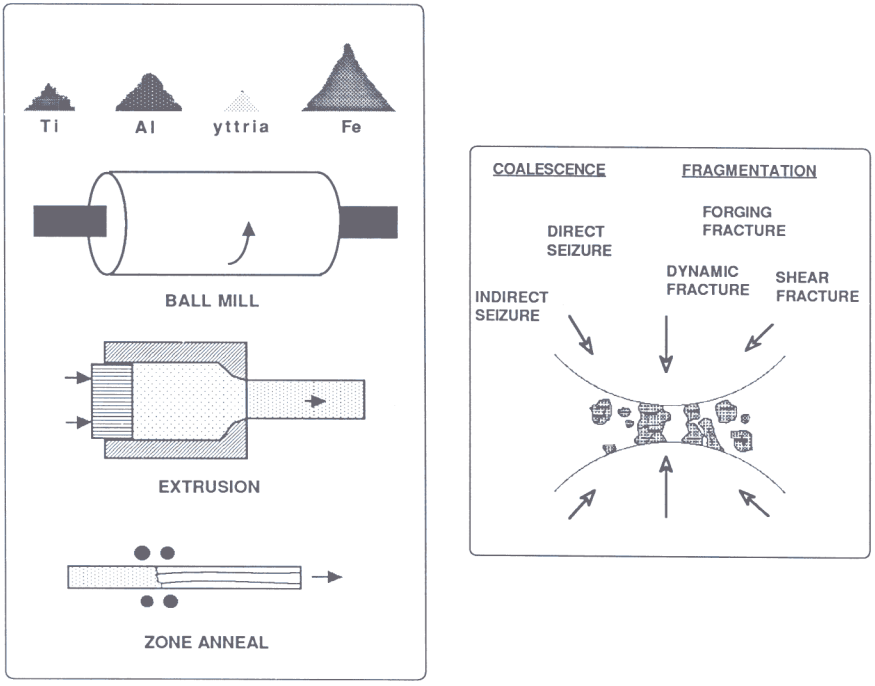

(a) (b)

Fig. 12. (a) Schematic illustrations of the mechanical alloying process. (b) The repeated fragmentation and coalescence of particles trapped between impacting balls leads eventually to solution during mechanical alloying (after Ref. 34). Dynamic fracture occurs during normal impact whereas the other processes are a feature of impact occurring in an inclined fashion.

a solution, it is said to be trapped.[31–33] Both of the elements are in this instant trapped, and the solution would never be expected to form spontaneously. There may nevertheless exist an industrial demand for such a solid solution, and mechanical alloying is a process which can enable this to happen for bulk samples.

5.2 *The Process*

Mechanical alloying is a process in which mixtures of fine powders consisting of elemental metals or master alloys are changed into solid solutions, apparently without any melting (Fig. 12).[34] The powders are forced to collide with each other and with much larger, hardened steel balls. The collisions are very energetic, involve large contact pressures, and lead

eventually to the formation of an intimate solid solution. The process can be carried out using a ball mill: in modern parlance, *a high energy attritor!* After manufacture, the mechanically alloyed powder is usually extruded to form full density bulk samples in rod, sheet or other useful shapes.

An advantage of mechanical alloying is that it can permit many thermodynamic constraints to solid or liquid solubility to be overcome, essentially by forcing elements into solution. Thus, large concentrations of aluminium can be incorporated into steels, in order to improve their oxidation and corrosion resistance. Rapid solidification is another technique which can help trap excessive concentrations of solute, but mechanical alloying does this without any melting. It can force normally incompatible materials to coexist on a fine scale.

After consolidation by extrusion, the alloys are usually extremely hard and possess an incredibly small grain size, typically a small fraction of a micrometer (Fig. 13). Such a small grain size is impossible to achieve by any other process for bulk samples. The material is usually extremely hard in the as-consolidated state, and has to be softened before further fabrication. The grain boundary area locked into the material gives it a large stored energy, which under suitable heat treatment conditions triggers recrystallisation into a much coarser grain structure. If annealing is carried out by passing the sample through a hot zone (zone annealing), then the recrystallisation front is localised within the high temperature region. The front then advances at the same rate as the sample, thereby leading to *directional recrystallisation* in which the microstructure consists of a series of very coarse columnar grains parallel to the zone annealing direction. It resembles in fact the microstructure obtained during directional solidification. The columnar grains are highly anisotropic, usually only restricted by the size of the sample, and can reach lengths in excess of a metre. In some instances, even isothermal annealing can lead to the development of columnar recrystallised grains. The reason for this needs investigation, but evidence is emerging that the yttria particles in the steel (introduced during mechanical alloying) are not isotropically dispersed, but are aligned parallel to the extrusion direction. Consequently, anisotropic Zener pinning of grain boundaries during isothermal recrystallisation may sometimes be the factor responsible for the development of a columnar grain structure.[35]

There are two main steels available commercially,[36] although there are numerous experimental alloys currently under investigation (Table 2). Both are ferritic stainless steels, one containing a large concentration (4.5 wt%) of aluminium in solid solution, together with about 0.5 wt% of yttrium oxide. The alloy is intended for oxidation and corrosion resistance, the yttria serving the purpose of maintaining a high strength at elevated temperatures. Amongst the major applications which could

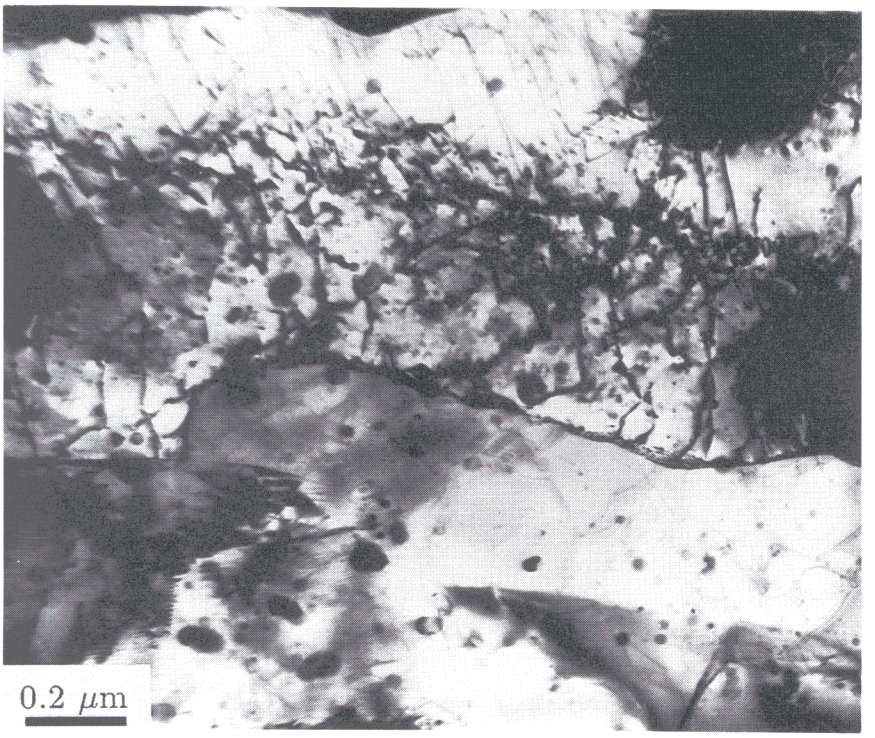

(a)

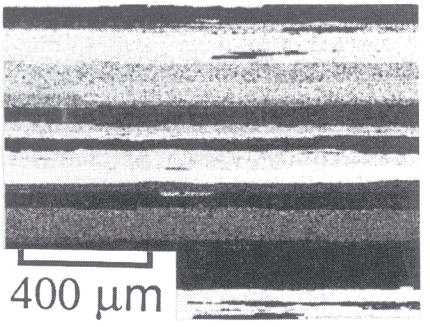

(b)

Fig. 13. (a) Transmission electron micrograph of a mechanically alloyed steel (MA956) after mechanical alloying and extrusion, showing the ultrafine grained microstructure. (b) Light micrograph illustrating the coarse columnar grain structure that develops during zone annealing of MA956.

come to fruition within the next decade, is one in small power generating plant designed to convert natural gas into electricity. There is a difficulty in joining these alloys without disrupting the microstructure, but explosive welding, solid-state bonding and mechanical joining techniques look promising.

The second mechanically alloyed steel is also ferritic. It contains yttria

Table 2 Chemical compositions (wt%) of mechanically alloyed steels

	C	Cr	Al	Ti	Mo	Y_2O_3
MA956	0.01	20	4.5	0.5	–	0.5
MA957	0.01	14	–	1.0	0.3	0.27

and about 1 wt% titanium and is destined for the nuclear power generation industry. The ferritic structure for some reason gives the alloy a low neutron capture cross-section, whereas the yttria again enhances the creep strength during high temperature service.

Although the processing and fabrication of these alloys needs much further investigation, the research to date is very promising indeed, and it is easy to imagine many useful applications.

6. Stress-corrosion Resistance by Design

Cleavage fracture occurs on a macroscopic scale when a critical stress is exceeded over a region ahead of a crack tip, leading to the propagation of a preexisting microcrack. The magnitude of this critical stress can be reduced drastically by environmental effects. In the context of high strength steels, embrittlement can follow directly from the infusion of hydrogen generated during corrosion reactions. Cleavage fracture thus occurs at a critical stress intensity K_{ISCC} that is generally much smaller than the limit K_{IC} defined in the absence of such environmental effects. The exact path followed by the cracks depends to some extent on the distribution of the hydrogen traps. For example, failure can be intergranular if carbide particles decorate the grain boundaries. The effects of grain boundary embrittling impurities and of hydrogen are known to be additive, so that for most high-strength steels the fracture path tends to be intercrystalline.[37]

The most probable mechanism for hydrogen embrittlement is that the hydrogen lowers the cohesion of the ferrite lattice.[37] When hydrogen enters a metal lattice, its nucleus (which is a single proton) is effectively screened by the 'gas' of delocalised electrons of the host metal. Thus, its bond with its own electron is weakened so that the hydrogen atom can easily ionise in the metal lattice at ambient temperature.[38] The 'size' of the hydrogen atom thus becomes miniscule. And yet, it causes an expansion of the ferrite lattice, indicative of a weakening of the Fe–Fe bonds.

For high strength steels, K_{ISCC} is usually found to be about a third of K_{IC}, so that stress corrosion can severely limit their effective use. The effect of corrosion manifests itself primarily via hydrogen embrittlement, the hydrogen being generated by cathodic reaction at the crack surface. It then diffuses to regions of highest dilatation ahead of the crack tip, leading to a reduction in the cohesive strength.[37,39–41]

The phenomenon of hydrogen stress corrosion can be very depressing to those involved in the design of high strength steels. Empirical observations (Fig. 14) show clearly that the resistance to stress corrosion cracking diminishes as the strength increases.[42] If this behaviour is accepted, then there is little point in designing very strong steels for structural applications. However, the correlation is based on conventionally designed steels. The section that follows discusses a radical and promising new approach.

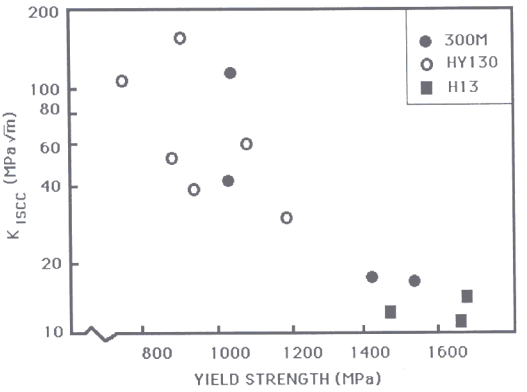

Fig. 14. The correlation of stress corrosion cracking resistance versus the yield strength for a variety of steels.[42]

6.1 Ni–Mo–La Steel

Manganese and silicon are two of the most common alloying additions made to steels. Nevertheless, it has now been demonstrated that large improvements in the grain boundary cohesion (and hence stress-corrosion cracking resistance) can be achieved by removing these elements.[43] The effects of stress corrosion cracking are also exaggerated by the presence of grain boundary embrittling elements such as phosphorus. The stress corrosion process is far more sensitive to such impurities when compared with temper embrittlement phenomena. Thus, the tolerable concentration of phosphorus is known to be at least an order of magnitude smaller in situations where the resistance to stress corrosion is paramount.[44]

A novel method for controlling phosphorus is based on the outcome of detailed thermodynamic calculations, which have suggested a most effective compound for the stable gettering of phosphorus,[44–46] Fig. 15. The compound is lanthanum phosphate ($LaPO_4$), which can be inuced to form if the liquid steel melt is highly undercooled. Further calculations suggest

that for the alloy studied, the concentrations of dissolved oxygen in equilibrium with lanthanum oxide (La_2O_3), lanthanum oxysulphide (La_2O_2S) and lanthanum phosphate ($LaPO_4$) are 2.8×10^{-7}, 6×10^{-9} and 1.7×10^{-3} wt% respectively, at a melt temperature of 1650°C. The tendency for the lanthanum to form oxides or oxysulphides is thus greater than to form the phosphate, which is not consequently found in slowly

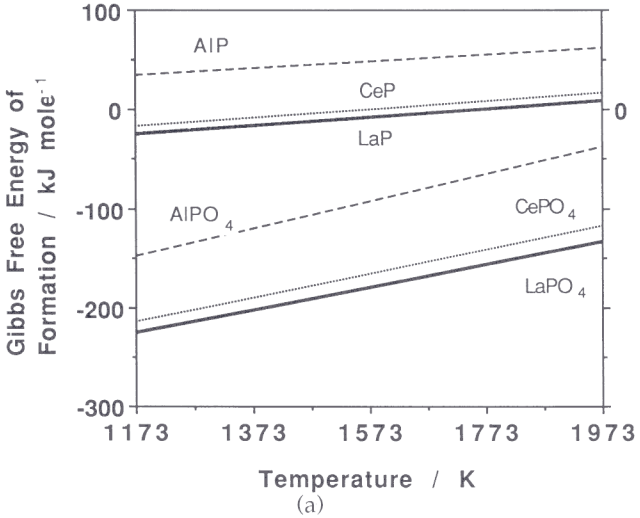

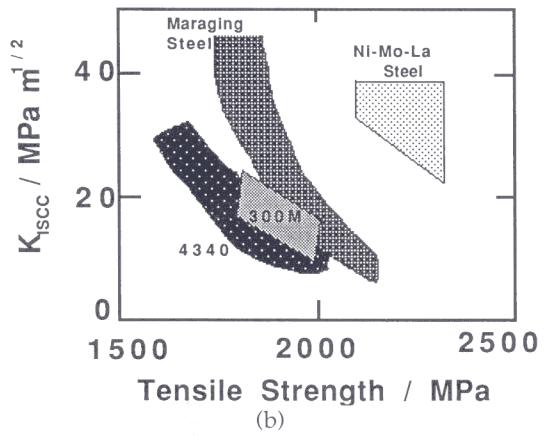

Fig. 15. (a) Free energies of formation of phosphorus compounds in liquid steel (data from Ref. 44). The free energy is per mole of metal, relative to the standard state 1 wt% solute in liquid steel at 1600°C (b) Stress-corrosion resistance as a function of yield strength, comparing the rapidly solidified 'Ni–Mo–La' steel against more conventional high strength steels widely used in industry.

cooled melts. If on the other hand, the melt can be rapidly cooled so that the oxygen in the liquid is supersaturated with respect to all three lanthanum compounds, then it becomes possible to getter the phosphorus.

Staggering enhancements of the stress-corrosion cracking resistance have been reported by using the above principles to design a steel containing lanthanum, which at the same time avoids other grain boundary embrittling elements such as manganese, silicon and chromium (Fig. 15b). The composition of the steel is thus Fe–0.4C–2Ni–1.5Mo wt%. The nickel and molybdenum are essential for hardenability, which is believed to be as high as that of AISI 4340 steel. The nickel concentration is typical of high strength steels, and in addition to its role in influencing hardenability, it also enhances the intrinsic toughness of the alloy. The carbon has a key role in boosting the strength of the martensite, the alloy being designed for use after mild tempering at 200°C.

The Ni–Mo–La steel described above is made by rapid solidification and consolidation of the resultant powder. The highly stable particles of lanthanum compounds have also been shown to stabilise the austenite grain structure during elevated temperature heat treatment.

7. Advanced Bainitic Steels

7.1 Calculation of Microstructure

One model for the bainite transformation in steels (Fig. 16) considers the growth of bainite to occur without any diffusion, but with the carbon redistributing from the ferrite into the residual austenite soon after transformation.[47] The partitioning of carbon can occur in a fraction of a second at the relatively high temperatures where bainite grows.[48] The precipitation of carbides occurs as a secondary reaction from the carbon enriched residual austenite for upper bainite. For lower bainite, the partitioning of carbon from supersaturated ferrite is relatively sluggish, so that an opportunity arises for some carbide precipitation within the bainitic ferrite.

Once this model is accepted, it becomes possible to go a long way towards a fairly complete calculation of the microstructure of many bainitic steels, including phase volume fractions, chemistries, etc. The calculations rely on the assumption in the model that the initial growth of bainite is diffusionless. Thus, austenite cannot transform into bainite if its carbon concentration exceeds that given by the T_O curve of the phase diagram (Fig. 16b). The T_O curve is the locus of all points on the phase diagram where austenite and ferrite of the same composition have identical free energies. The T'_O curve also allows for the strain energy due to the displacive transformation mechanism. The maximum volume fraction of bainitic ferrite that can be achieved during isothermal transformation is

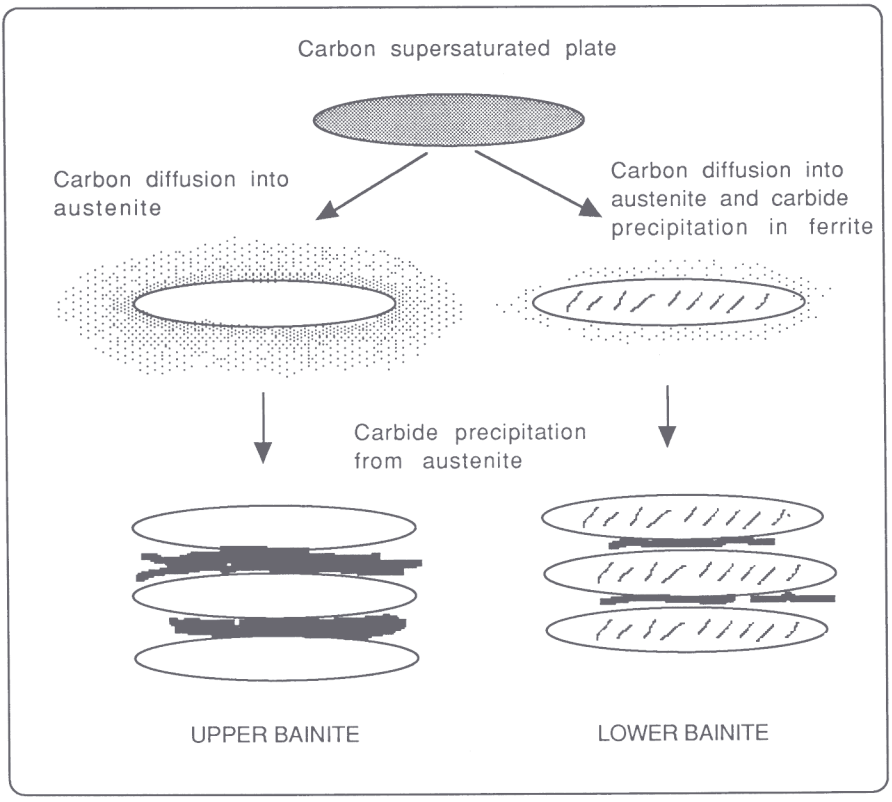
Carbon supersaturated plate
Carbon diffusion into austenite
Carbon diffusion into austenite and carbide precipitation in ferrite
Carbide precipitation from austenite
UPPER BAINITE
LOWER BAINITE

(a)

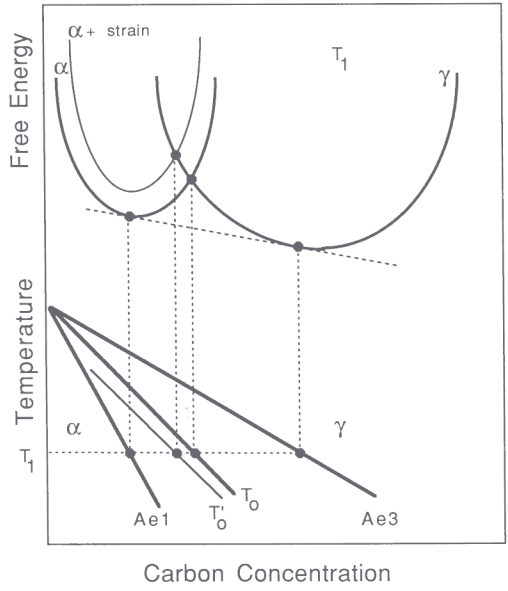
α + strain
α
T1
γ
Free Energy
Temperature
α
γ
T1
Ae1
T'o
To
Ae3
Carbon Concentration

(b)

therefore not given by the application of the lever rule to the equilibrium or paraequilibrium phase boundaries, but by the point where the level of carbon in the austenite reaches a value given by the T'_O curve. This concept is the essential feature of all modern calculations of bainitic microstructures, and is currently being utilised in many industries all over the world in the design of high strength steels. Two examples are given below.

7.2 Alloy Design: Carbide-Free Bainitic Steels

Bainite was discovered, as a microstructure in its own right, in the late 1920s by Davenport and Bain[49] during the course of some pioneering studies on the isothermal transformation of austenite. It was the cause of much excitement because the bainitic samples seemed to display unusual and promising properties. Bain, in 1939[50] went so far as to suggest that the microstructure was found to be 'tougher for the same hardness than tempered martensite'.

In spite of this early optimism, many years elapsed before any major commercial exploitation of bainitic steels. There were difficulties in obtaining fully bainitic microstructures in sizeable samples of steel. Industry also preferred continuous cooling heat treatments, and at rates which could not in practice exceed ~ 50°Cs^{-1}. In these circumstances, lean steels gave mixed microstructures of allotriomorphic ferrite and bainite, whereas the more heavily alloyed steels transformed only partially to bainite, some of the residual austenite undergoing martensitic transformation on further cooling. It was not until low-alloy, low-carbon steels, containing small amounts of boron and molybdenum to suppress allotriomorphic ferrite formation were developed by Irvine and Pickering[51–52] in the late 1950s, that the potential for significant commercial exploitation became realistic. Boron increases the bainitic hardenability. Other solute additions can, in the presence of boron, be kept at sufficiently low concentrations to avoid the formation of martensite. Steels like these were found to yield virtually fully bainitic microstructures with very little martensite during normalising heat treatments. The steels exhibited reasonable combinations of toughness and strength, but in time proved to be unexciting when compared with the best of quenched and tempered martensitic steels. By contrast, there has been a remarkable turnaround in the fortunes of bainitic steels over the past ten years, with the exploitation of alloys which do not contain any carbides.[53] It is not an

---

Fig. 16. (a) Schematic illustration of the mechanism of bainitic transformation in steels. (b) Free energy curves illustrating the T_O curve on the phase diagram.

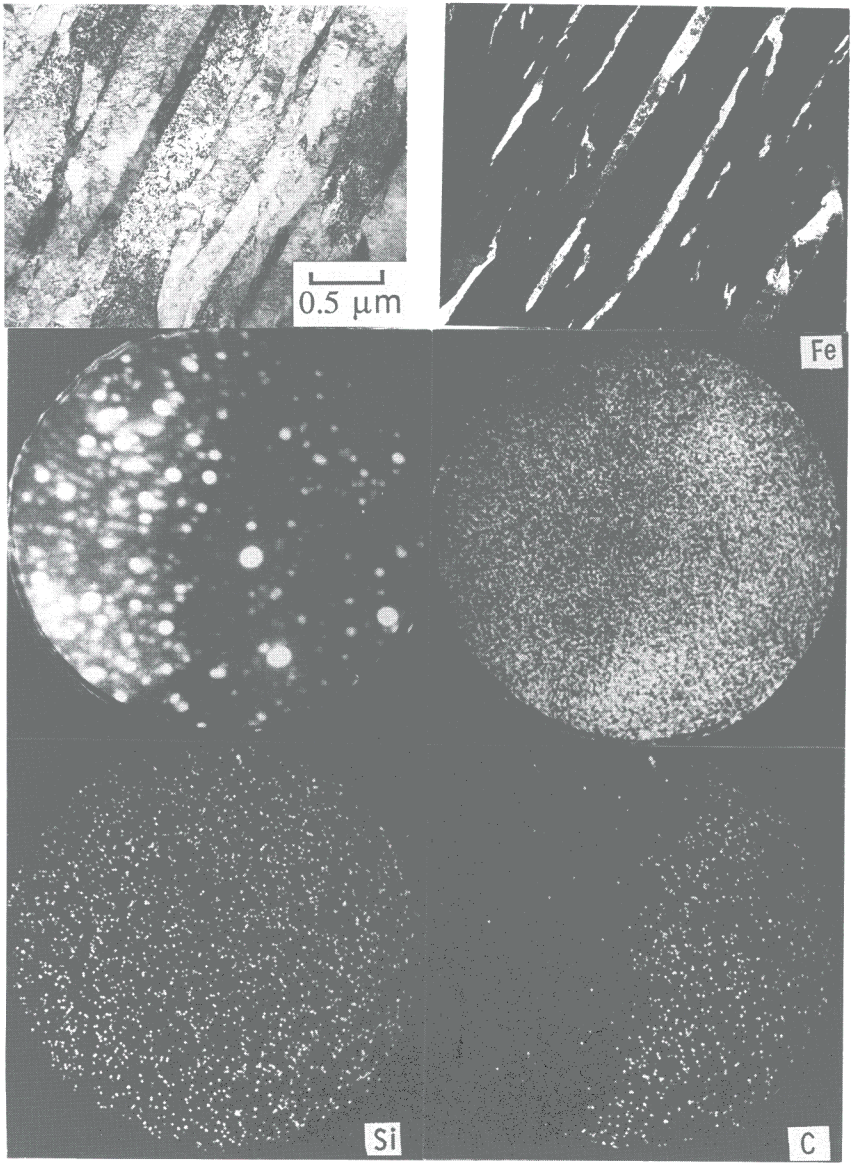

Fig. 17. (a) Transmission electron micrograph of a mixture of bainitic ferrite and stable austenite (b) corresponding austenite dark field image (c) a field ion image (middle left) showing the atoms of bainitic ferrite on the left hand side, and those of austenite on the right hand side. The other three images are obtained from the same region, and illustrate the distribution of Fe, Si and C. Note that the austenite is carbon-rich, but that substitutional solutes do not partition between the phases, even on the finest conceivable scale (after Ref. 54).

exaggeration to say that these alloys account for a large proportion of the major new developments in steel technology, and are the subject of numerous research programmes.

It is now well established that in many steels, and especially those with large concentrations of silicon or aluminium in solid solution, the carbide precipitation reactions normally associated with bainite lag far behind the growth of bainitic ferrite.[47] As a consequence, the carbon which is rejected from the bainitic ferrite enriches the residual austenite, thereby stabilising it to martenistic transformation during cooling to ambient temperatures (Fig. 17).

The mixture of bainitic ferrite and austenite is in principle an ideal combination from many points of view. Most modern high strength steels are clean in the sense that they are largely free from nonmetallic inclusions. Those destined for critical applications are usually vacuum arc refined prior to fabrication and heat treatment. As a consequence, it is the intrinsic components of the microstructure, such as particles of cementite, which are responsible for damage initiation. The upper bainitic ferrite and austenite mixture is, however, free from cleavage and void nucleating cementite. The ferrite also has a very low interstitial content, since much of the excess carbon is partitioned into the residual austenite; the toughness of ferrite is known to deteriorate rapidly with an increasing concentration of carbon in solid solution.

The microstructure derives its strength from the ultrafine grain size which results from the displacive mechanism of ferrite growth, giving an effective grain size which is much less than 1 μm. Such a small grain size cannot be achieved by any commercial process other than mechanical alloying (a powder metallurgical process). A fine grain structure is an optimum method for improving strength since unlike most other strengthening mechanisms, the improvement in strength is also accompanied by an improvement in toughness. The intimately dispersed and ductile FCC austenite films between the ferrite platelets can be expected at the very least to have a crack blunting effect, and could also increase the work of fracture by undergoing martensitic transformation under the influence of the stress field of the propagating crack (i.e. the TRIP, or transformation induced plasticity effect). The diffusivity of hydrogen in austenite is relatively sluggish, so that its presence might enhance stress corrosion resistance. And all these potential benefits can be achieved by creating a duplex microstructure with the cheapest austenite stabiliser available, carbon, whose concentration in the austenite is enhanced during transformation, so that the average carbon concentration of the steel need not be large.

In spite of all these potential advantages, the bainitic ferrite/austenite microstructure has on many occasions failed to live up to expectations, primarily because of the instability of relatively large or blocky regions of

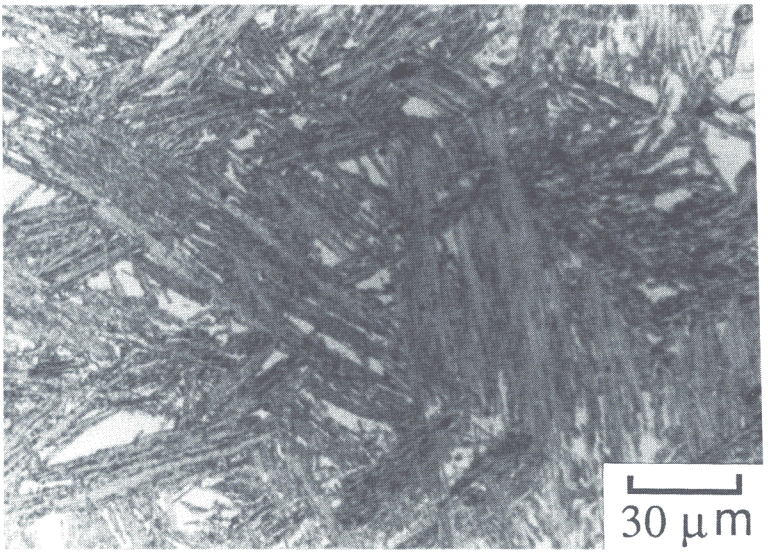

(a)

(b)

(c)

austenite which become trapped between the sheaves of bainite (Fig. 18). The blocks of austenite tend to transform to high-carbon, untempered martensite under the influence of small stresses and consequently have an embrittling effect. The films of austenite that are trapped between the platelets of ferrite in a sheaf are much more stable, partly because of their higher carbon concentration, and also because of the physical constraint to transformation due to the close proximity of plates in all directions.

If it is assumed that a fraction ϕ of a sheaf consists of films of austenite, then it can be demonstrated that the ratio of the volume fractions of film and blocky austenite (prior to any martensitic transformations) is given by

$$\frac{V_{\gamma\text{-}F}}{V_{\gamma\text{-}B}} = \frac{\phi V_\alpha}{V_\gamma - \phi V_\alpha} \tag{6}$$

where $V_{\gamma\text{-}F}$ and $V_{\gamma\text{-}B}$ are the volume fractions of film and blocky type retained austenite respectively, and V_α and V_γ the total volume fractions of bainitic ferrite and residual austenite respectively. It is found experimentally that high strength and good toughness can be obtained by maintaining the above ratio to a value greater than 0.9.[55,56] The question then arises as to the factors which control this ratio.

7.3 Optimisation

Theory suggests three different ways of minimising the volume fraction of blocky austenite, each involving an increase in the total volume fraction of bainitic ferrite.[55,56]

A reduction in the transformation temperature permits the bainite reaction to proceed to a greater extent but there is a limit to the minimum transformation temperature since the lower bainite and martensite reactions eventually set in. An increase in the extent of reaction can also be achieved by reducing the overall carbon concentration of the steel, so that the austenite reaches its limiting composition at a later stage of the reaction. The T'_O curve of the phase diagram, which determines the composition of the austenite at the point where the reaction stops, can also be

---

Fig. 18. (a) Optical micrograph of upper bainite Fe–0.43C–3Mn–2.02Si wt% alloy transformed isothermally at 295°C for 115 minutes before cooling to ambient temperature. Illustrates the blocks of retained austenite between sheaves of bainite (b) and (c) Bright field and retained austenite dark field electron micrographs of the same sample after stressing to 850 MPa in tension, showing that the larger regions of austenite transform to martensite but the films are preserved as austenite.

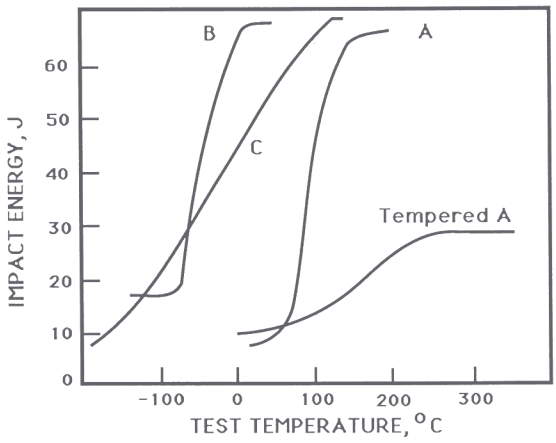

(a)

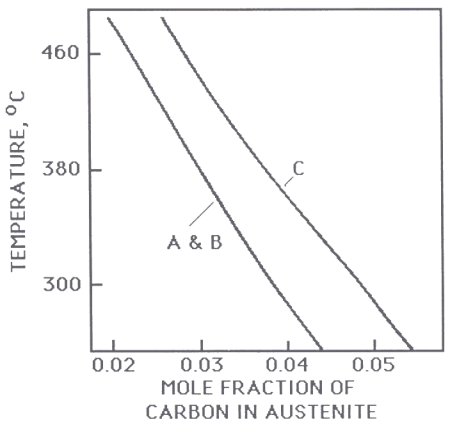

(b)

Fig. 19. (a) Impact transition curves demonstrating how the toughness can be improved, without a loss of strength, simply by minimising the amount of blocky austenite in a mixed microstructure of bainitic ferrite and austenite. Curve A refers to upper bainite in a Fe–0.43C–2Si–3Mn wt% alloy for which the film to blocky austenite ratio is 0.5. Curve B is for a similar alloy but with about half the carbon concentration. Curve C represents an alloy with the same carbon concentration as A but with the manganese replaced with 4 wt% nickel in order to shift the T'_O curve to higher carbon concentrations. The film to blocky austenite ratio is greater than 1.5 for alloys B and C. (b) T'_O curves for alloys A, B, and C.[55,56]

shifted to higher carbon concentrations by altering the substitutional solute concentration of the steel. The effect on toughness in reducing the amount of blocky austenite is shown in Fig. 19a, which illustrates the large changes in the impact transition temperatures as the ratio of film to blocky austenite is increased in the manner just described. Note that for a duplex ferrite plus austenite microstructure, the strength actually increases as the fraction of bainitic ferrite increases, so that better toughness is obtained without sacrificing strength.

Typical compositions of high strength steels which show good toughness are given in Table 3. Figure 20 shows how the mechanical properties compare with quenched and tempered steels. It is evident that in some cases, the properties match those obtained from the much more expensive marageing steels.

Table 3 Chemical compositions (wt%) of experimental high strength steels with microstructures consisting of mixtures of bainitic ferrite and retained austenite

C	Si	Mn	Ni
0.22	2.0	3.0	–
0.40	2.0	–	4.0

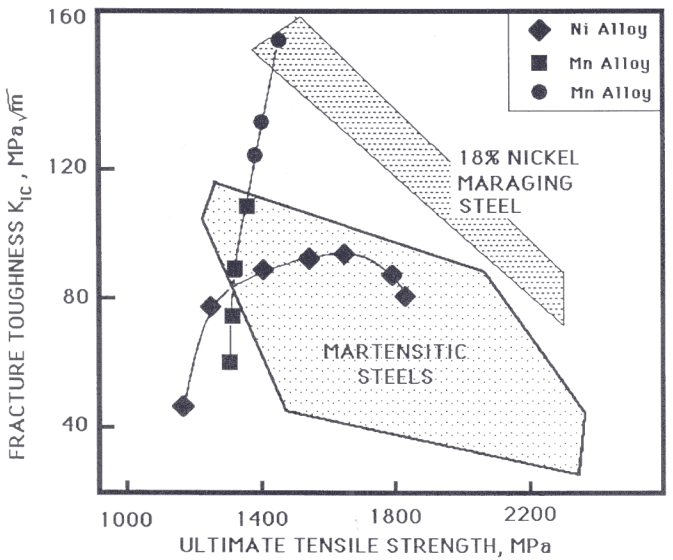

Fig. 20. Comparison of the mechanical properties of mixed microstructures of bainitic ferrite and austenite, versus those of quenched and tempered martensitic alloys.[57]

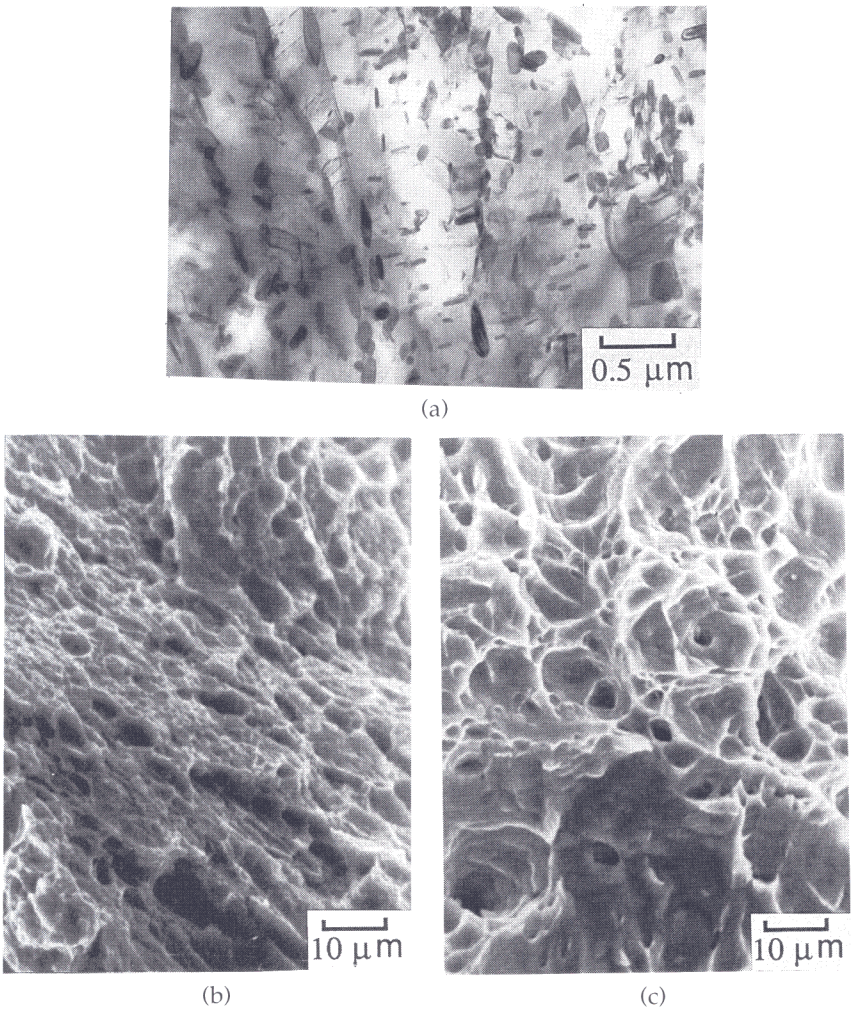

Fig. 21. (a) Microstructure of carbides and ferrite, obtained by tempering bainitic ferrite and austenite at 615°C. Comparison of the fracture surfaces of tempered (b) and untempered (c) samples, from impact samples tested in the upper shelf region.

The properties of these 'silicon steels' improve only slightly when tempered at temperatures not much higher than the transformation temperature at which the original bainite formed. However, annealing at elevated temperatures or prolonged periods at low temperatures can lead to the decomposition of the austenite into ferrite and carbides, with a

simultaneous drop in strength and toughness, especially the upper shelf energy (Fig. 21). The latter effect can be attributed directly to the void nucleating propensity of carbide particles in the tempered microstructure, as illustrated by the much smaller void size evident in the fracture surface of the tempered sample (Fig. 21c).

The mechanical property data on these high silicon steels, especially those steels designed using the phase transformation theory discussed earlier, look extremely promising. It is unlikely that even these alloys represent the optimum compositions, so that further improvements are possible. A more comprehensive assessment of properties such as stress corrosion resistance, fatigue etc. is also needed.

7.4 Hard Bainitic Rail Steels

Modern railway tracks are subjected to intense use, with relatively fast trains and increasing axle loads. Rails must consequently be more wear resistant, and achieve higher standards of straightness and flatness in order to avoid the sort of surface and internal defects which may eventually lead to failure.

Wear is a system property, not a material property. The relationship between microstructure and wear properties is known to be tenuous. The most prominent correlation is that the wear rate decreases monotonically with the hardness of the microstructure, although exceptions to this rule have also been reported.[58] Apart from hardness, other features of the microstructure must have additional influences on the wear behaviour, albeit to a lesser extent when compared with the sensitivity to hardness. The microstructural effect is emphasised by the established fact that in the context of rails, a refinement of microstructure can prolong the wear-limited rail life.[59]

Railway steels therefore have to be strong (hard) in order to be wear resistant. They have conventionally been based on high carbon steels of near eutectoid composition and pearlitic microstructures. It is the carbide phase which is crucial in providing the necessary hardness. A novel approach towards the longer term development of wear resistant and much tougher rail steels has been based on medium carbon bainitic alloys *without any carbides!* Rail steels designed with the bainitic ferrite and austenite duplex microstructure have already demonstrated wear resistance significantly better than conventional alloys, including conventional heat treated steels (Fig. 22). A typical composition for the new steel is Fe-0.5C-1.5Si-2.0Mn wt% the chemistry being decided using thermodynamic and kinetic theory for bainitic transformations.[60] The hardness in the duplex microstructural condition is about 400 HV. Some of the other measured properties also turn out to be better than currently

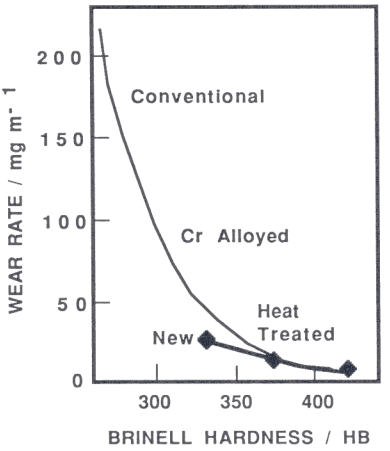

Fig. 22. Comparison of the wear rates and hardness levels of conventional rail steels versus the new alloys which have a carbide-free microstructure of bainitic ferrite and austenite.

available rail steels, but the details are at the moment commercially sensitive. Further development work, guided by fundamental research is now in progress to bring this concept to fruition.

7.5 Retained Austenite and Stress Corrosion

As emphasised before, stress corrosion can severely limit the performance of high strength steels. There are good intuitive arguments to suggest that retained austenite could be beneficial in this respect, although as discussed below, it is certainly not a panacea for all of the problems associated with strong steels. More research is needed in this area, and so an attempt is made here to assess the role of retained austenite, which occurs in profusion in bainitic steels, in determining stress corrosion properties.

It is difficult to comment on the relationship of K_{ISCC} with microstructure (and very few data exist for bainitic microstructures) but it appears that the presence of retained austenite reduces the stress corrosion crack growth rate, by hindering the diffusion of hydrogen to the sites of triaxial tension ahead of the advancing crack front.[61,62] The bulk diffusivity of hydrogen through austenite can be many orders of magnitude smaller than that in ferrite.[63] Comparative experiments on tempered martensite and on a mixed microstructure of lower bainite, martensite and retained austenite (of the same yield strengths as the tempered martensite) revealed that the sample containing the larger quantity of austenite exhibited better stress corrosion resistance in a NaCl solution.[62] While both

samples showed intragranular failure with respect to the prior austenite grain surfaces, a greater proportion of ductile tearing was found at those surfaces for the bainitic samples. This was attributed to the ability of the retained austenite to act as sinks for impurities,[64] thereby leading to a lower degree of embrittlement at the grain boundaries. It is well established that prior austenite grain boundary embrittlement effects lead to higher stress corrosion crack growth rates.[65]

Whilst these investigations emphasise the role of retained austenite in enhancing stress corrosion resistance, some recent work[42,66] has stressed that there are restricted conditions under which the austenite can be beneficial. For example, the austenite has to continuously surround the plates of ferrite if it is to significantly hinder the diffusion of hydrogen. The role of austenite also does not appear to be as prominent as has been suggested by earlier investigations; other microstructural modifications which led to a high density of innocuous hydrogen traps (e.g. interfaces between cementite and ferrite) were often found to cause larger improvements in stress corrosion resistance.

In fact, Kerr *et al.*,[66] and Solana *et al.*,[42] studied a wide range of microstructures in high strength steels and were able to establish some general principles relating them to stress corrosion resistance (SCR). The sensitivity to microstructure was largest at yield strengths less than about 1000 MPa, and when failure occurred by a transgranular mechanism. Furthermore, the largest improvements obtained did not correlate with the presence of retained austenite. For reasons which are not clear, twinned martensite was deleterious to SCR; this may have something to do with the fact that in the steels studied, twinned martensite is usually a high carbon martensite (and hence more brittle), the twins themselves being inconsequential to the SCR problem. Mixtures of ferrite and martensite were found to be better, correlating with extensive crack branching due to the numerous interphase interfaces. The presence of lower bainite also led to improved SCR, but the effect could not be separated from any effect due to the associated drop in yield strength. All other factors being equal, reductions in yield strength correlated strongly with improved SCR. Alloy specific effects were also observed, and attributed to differences in the density of innocuous traps for hydrogen. Indeed, any feature of the microstructure which enables the hydrogen to be well dispersed, or which promotes crack branching, seems to lead to improved SCR in steels where the role of hydrogen is crucial.

8. Harder than Martensite?

There are now considerable data that the presence of bainite in a predominantly martensitic microstructure enhances both strength and

toughness relative to the single phase samples.[67,72] For example, the strength of a mixture of lower bainite and martensite in an isothermally transformed high strength steel has been found to go through a maximum as a function of the volume fraction of lower bainite (Fig. 23). This goes against intuition in that the overall strength of a two phase microstructure may be expected to be between that of the individual phases in isolation. The results were explained using an idea proposed by Mutui *et al.*[73] The bainite subdivides and thus refines the austenite grain structure prior to martensitic transformation. Martensite in low alloy steels tends to form in packets whose size is related to that of the austenite grain structure, so that the packet size is refined. This leads to a strengthening of the martensite via a Hall–Petch effect. In addition, the strength of the bainite is supposed to be enhanced by the constraint provided to its deformation by the stronger martensite.

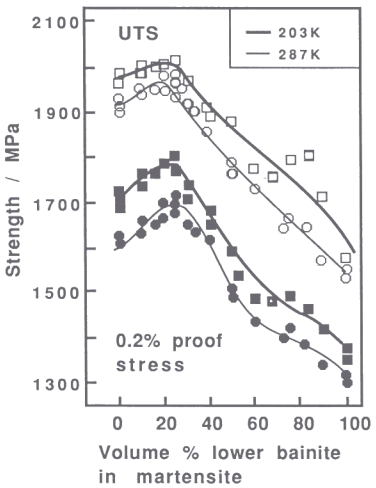

Fig. 23. Variation in the 0.2% proof stress as a function of the volume fraction of lower bainite in a mixed, tempered microstructure of lower bainite and martensite. The different curves represent data collected at the temperatures indicated on the diagram.

The details of the explanation of enhanced strength are not really satisfactory, but the experimental data are clear. The overall strength of a mixture of lower bainite and martensite certainly can exceed that of the martensite alone, and yet leads to an improvement in toughness (Fig. 24). This latter improvement was initially ascribed to the cleavage–crack stopping ability of the more ductile lower bainite, but fractography revealed a ductile fracture mechanism rather than regions of quasicleavage where

the martensite fractures in a brittle manner, separated by ductile fracture in the lower bainitic areas.[71] The notion that the dispersal of a ductile phase in an otherwise brittle matrix leads in itself to an improvement in properties is most likely an oversimplification, since mixtures of upper bainite and martensite do not lead to any improvement in toughness. Similarly, correlations of fracture facet size against microstructural parameters have not revealed any clear explanation for the change in fracture mode or toughness. Apart from the obvious refinement of martensitic regions in the mixed microstructures, any strength/toughness relationship must include the well established fact that the bainitic carbide particle size is much smaller in lower bainite when compared with upper bainite.

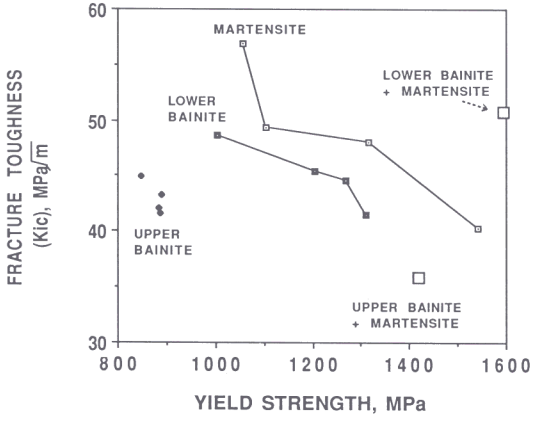

Fig. 24. Plot of toughness versus strength for a variety of microstructures in an ultrahigh strength steel [data from Ref. 72].

9. Chaotic Microstructures

There is frantic activity in the steel industry on the subject of 'acicular ferrite', which is essentially intragranularly nucleated bainite. The heterogeneous nucleation sites are known to be nonmetallic inclusions, either added deliberately, or present as impurities. The microstructures of conventional bainite and acicular ferrite differ significantly: clusters of bainite plates (called sheaves) grow as a series of parallel plates in identical crystallographic orientation emanating from austenite grain *surfaces*, whereas acicular ferrite plates nucleate intragranularly at *point* sites so that parallel formations of plates cannot develop (Fig. 25). It is widely

believed that the toughness is enhanced when the plates do not form packets, but point in many different directions like acicular ferrite. The feeling is that the latter microstructure causes the cleavage cracks to frequently deflect since new crystallographic orientations are presented each time a new plate is encountered.

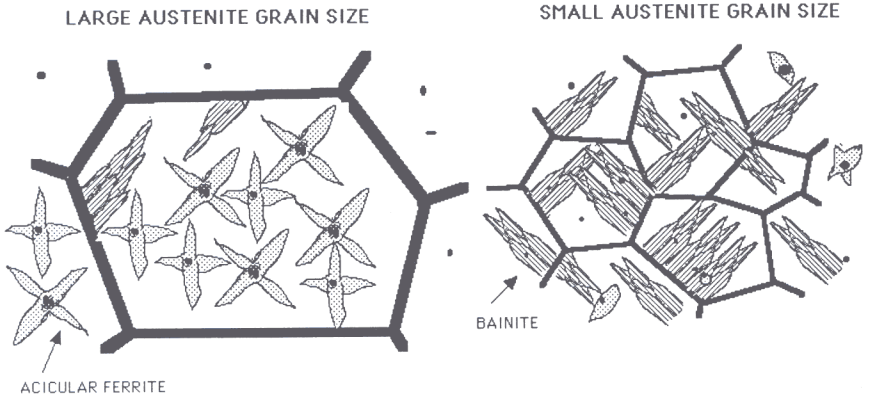

Fig. 25. Schematic illustration of the sheaf structure of bainite, and the individual platelets of acicular ferrite.

The dismantling of packets of parallel ferrite plates in bainitic or martensitic microstructures, into more chaotically orientated acicular ferrite plates, improves toughness. The increased chaos can only be achieved by introducing inclusions as intragranular nucleation sites. The greatest success in inducing the formation of acicular ferrite in this way has been achieved in weld deposits, which under normal circumstances contain relatively large concentrations of trace elements such as oxygen (about 300 ppm), aluminium, titanium, *etc.* introduced during fusion. The gain in toughness achieved in this manner seems to overcome any loss due to the presence of inclusions, in welds and low-strength steels. The same concentration of inclusions cannot however, be tolerated in ultrahigh-strength steels ($\sigma_Y \geq$ 1300 MPa) which typically contain oxygen at < 20 ppm.

The problem can be overcome once it is realised that it is not so much the absolute concentration of inclusions that matters, but the relative number densities of grain boundary and inclusion nucleation sites, for bainite and acicular ferrite respectively. A bainitic microstructure can be converted to one which is predominantly acicular ferrite by reducing the austenite grain surface per unit volume. One way of eliminating the austenite grain surfaces as potential nucleation sites is by decorating them with a very thin layer of allotriomorphic ferrite. The very small oxygen concentration present in an ultra high strength steel is then sufficient to induce the formation of intragranularly nucleated ferrite plates (Fig. 26).[74]

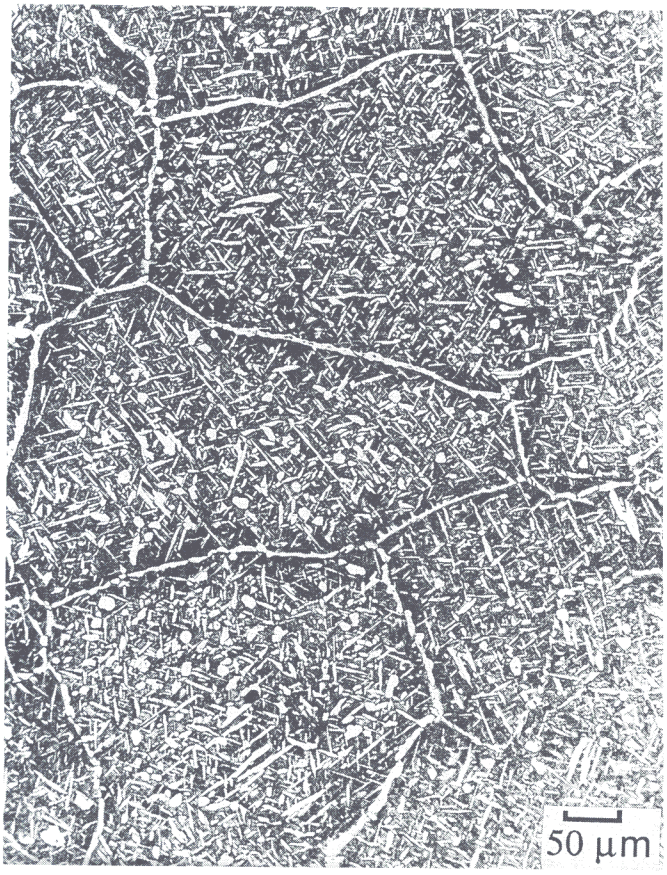

Fig. 26. Optical micrograph showing intragranularly nucleated Widmanstätten ferrite plates in an ultra-high-strength-steel containing only 40 ppm of oxygen.[74]

9.1 The Effect of Stress

We consider here how stress might influence the development of chaotic microstructures in the context described above. All of the transformations of interest in high strength steels, i.e. Widmanstätten ferrite, bainite, acicular ferrite and martensite are displacive in that their growth is accompanied by an invariant-plane strain shape deformation with a large

shear component (Fig. 27). The transformation can be regarded as a deformation which not only causes a change in shape, but unlike mechanical twinning and slip, also causes a change in the crystal structure of the deformed region; furthermore, the deformation can in this case be driven by a chemical driving force as the parent phase is undercooled below an equilibrium transformation temperature.[75,76]

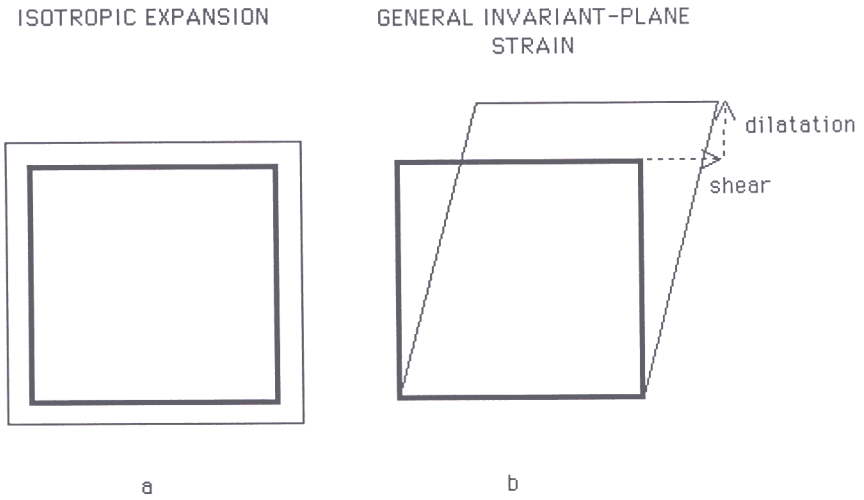

Fig. 27. Schematic illustrating of two particular changes in shape during transformation. (a) An isotropic volume expansion. (b) A general invariant-plane strain shape deformation with both a dilatational component (normal to the habit plane) and a large shear component (parallel to the habit plane).

Given that displacive transformations in steels cause considerable deformation, it follows that an external stress can influence the development of such transformations. This is illustrated in Fig. 28, where a fine grained polycrystalline sample of austenite was stressed at a temperature above its martensite start temperature.[77] The amount of martensite obtained varies directly with the magnitude of the applied stress (i.e. the mechanical driving force). Not only did the stress induce the formation of martensite, but only those particular variants of martensite which complied with the applied stress grew in profusion. Thus, most of the plates attempted to grow on planes close to those of the maximum shear stress (approximately 45° to the tensile axis).

In the absence of an externally applied stress, each austenite grain could have transformed into one or more of the twenty-four possible crystallographic variants, leading to a more chaotic microstructure. The stress caused the alignment of plates, and a more ordered microstructure.

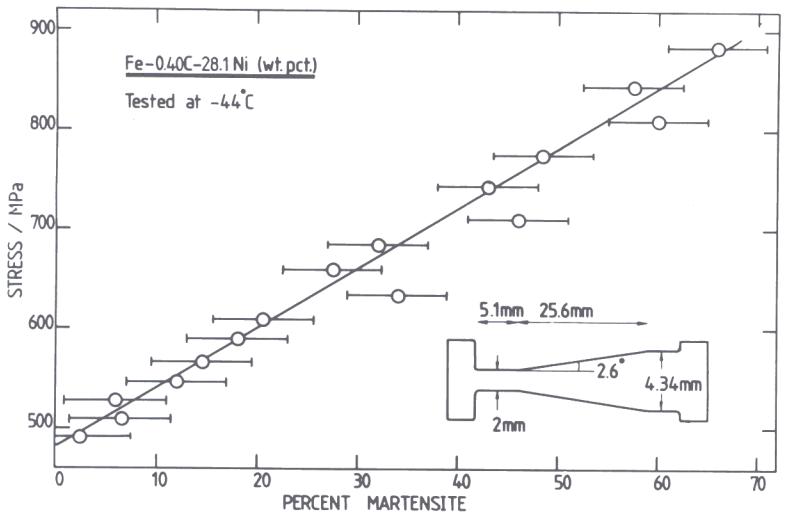

(a)

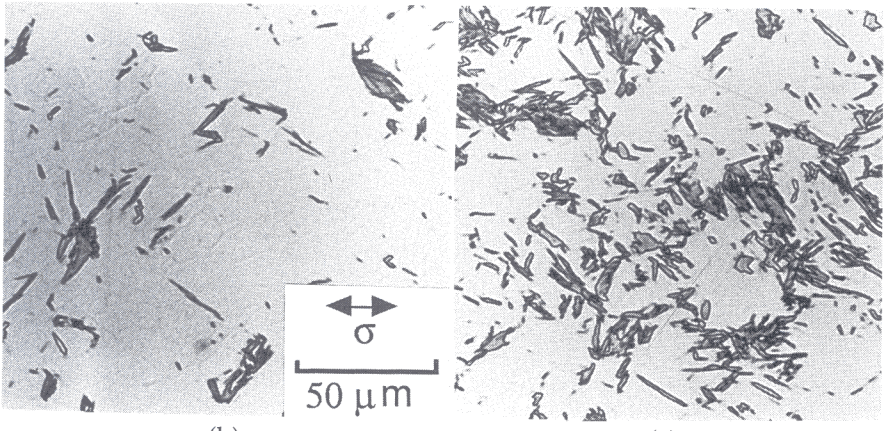

(b) (c)

Fig. 28. Stress induced martensitic transformation in a Fe–28Ni–0.4C wt% alloy tested at a temperature above the martensite start temperature (a) Volume fraction of martensite as a function of stress. (b) Optical micrograph from a low stress region (c) Optical micrograph from a high stress region. The arrow indicates the direction of the tensile stress.[77]

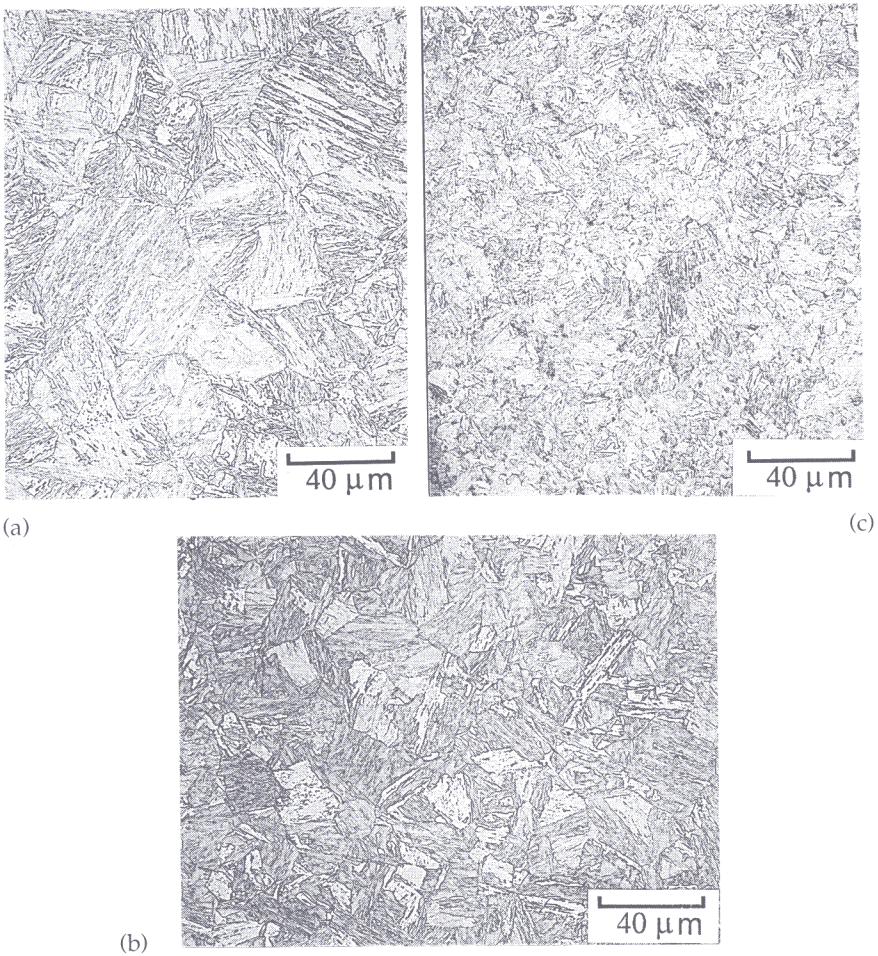

Fig. 29. Light micrographs of bainitic microstructures generated by isothermal transformation under the influence of stress within the range 0–95 MPa. The stress axis is horizontal in each of the micrographs, and the heat-treatment is identical for all the samples. (a) After transformation at 400°C at zero stress. (b) After transformation at 400°C under the influence of a tensile stress of 45 MPa. (c) After transformation at 400°C under the influence jof a tensile stress of 95 MPa.[78]

Figure 29 shows the results of bainitic transformation under the influence of an externally applied stress, which should favour the development of variants whose shape deformations comply with the imposed stress system. The austenite grain size in each of the micrographs illustrated is

identical, and yet a comparison of the zero and high stress samples shows quite different microstructures. Each austenite grain appears to transform to fewer variants as the stress is increased, giving a much more blocky and ordered microstructure. Thus, stress favours the formation of parallel plates (within the blocks) rather than the more chaotic microstructure evident in Fig. 29a. This must have significant implications on mechanical properties, a subject yet to be investigated.

10. Mechanically Homogeneous Weld Deposits

In many industrial applications, components are joined by depositing liquid metal using welding techniques, with several successive layers of molten metal required to fill the weld gap. The heat input due to the deposition of each layer in turn heat treats all the underlying regions, thereby causing local changes in microstructure and mechanical properties. There is growing evidence that the mechanical and microstructural inhomogeneity of the type associated with multirun welds causes *scatter* in properties.[79] For toughness, the lower bound within the scatter has to be accepted for design, leading to a less than optimum exploitation of material properties. The problem can be circumvented in single run welds but the large heat input required leads in many cases to unacceptable quality. Tempering treatments or weld refinement techniques can induce mechanical homogeneity but at the expense of mean strength.

A novel method has been suggested, aimed at the production of homogeneous multi-run welds of high strength and toughness, with a microstructure of acicular ferrite and ductile martensite. It requires the simultaneous satisfaction of four conditions:

1. The Ae_3 temperature of the weld metal should be reduced, so that the effect of depositing a new layer is to reaustenitise as much of the adjacent substrate as is possible.[80,81]
2. The hardenability must be adjusted to permit the reaustenitised regions to transform back on cooling to a microstructure consisting of the required mixture of acicular ferrite and ductile martensite.
3. A low Ae_3 also ensures that reheated regions which are not reaustenitised, do not undergo excessive tempering (to avoid a loss of strength). The alloy concerned must therefore be resistant to tempering.
4. The strength of acicular ferrite is a limiting factor and must be enhanced by the presence of martensite. A low average carbon concentration is essential to ensure ductile martensite. Unusually, the fraction of acicular ferrite must be kept small (~ 0.5) to avoid excessive austenite carbon enrichment which could otherwise embrittle the martensite.

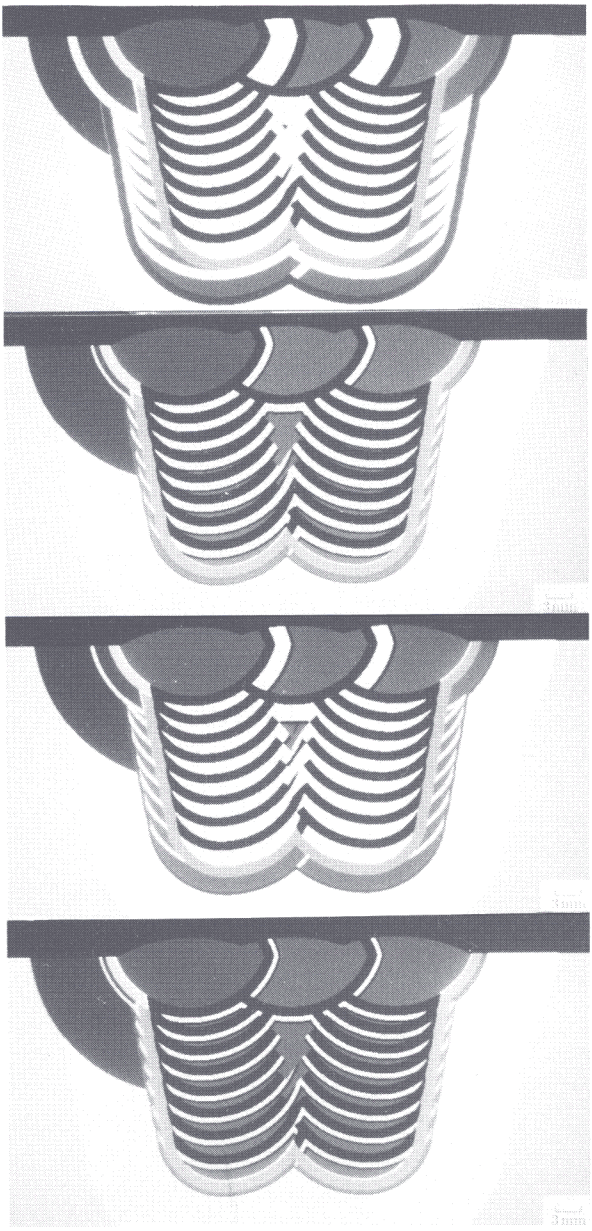

Fig. 30. Computer model of a typical multirun steel weld deposit. The colours represent different thermal histories, but the crimson colour is the one identified to lead to the weakest microstructure, and contribute most to mechanical heterogeneity. Its area fraction clearly decreases as the Ac_3 temperature is reduced (a–d).[82]

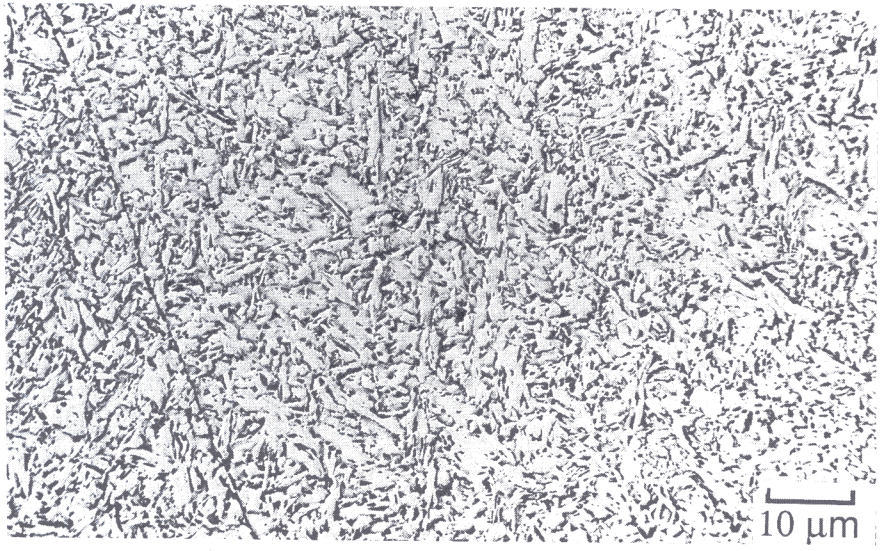

(a)

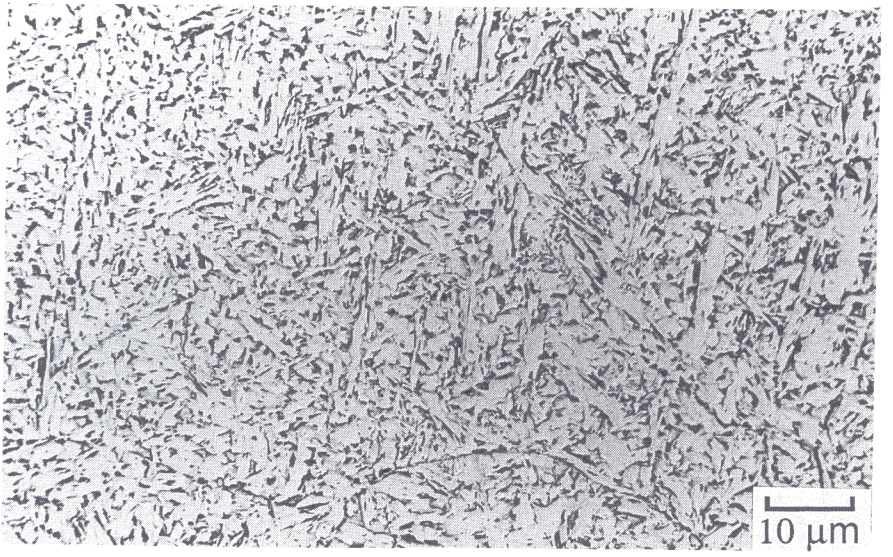

(b)

Fig. 31. Scanning electron micrographs illustrating the unusual uniformity of microstructure in a weld designed for microstructural and mechanical homogeneity. (a) As-deposited region. (b) Region reheated by the deposition of another layer.

Item 1 has already been verified by calculations, as illustrated in Fig. 30.

Tentative results from experiments designed to verify the calculations[83] have already demonstrated very high strength welds with almost identical microstructures in the as-deposited and reheated regions (Fig. 31).

11. Conclusions

The examples discussed above represent just a few of the recent developments in the physical metallurgy of high strength steels. The success of these and many other examples of steel metallurgy depends both on systematic academic research, and the determination of industry to invest in, and exploit the ideas. Whatever else the future holds, Sir Robert Honeycombe can be certain that steels will remain at the forefront of materials science and technology.

12. Acknowledgements

I am grateful to Professor C. Humphreys for the provision of laboratory facilities at the University of Cambridge. I am also grateful to Drs R.R. Preston and V. Jerath for allowing me to incorporate some of the unpublished information from our collaborative work on rail steels. I appreciate the kindness of Dr T. Inoue and his colleagues at Kobe Steel, who introduced me to Scifer, and provided me with several micrographs and other data. Some of the work presented here was carried out under the auspices of the Atomic Arrangements: Design and Control Project, which is a collaborative venture between the University of Cambridge and the Japan Research and Development Corporation.

References

1. C. Zener, *J. Appl. Phys.* **22**, 372, 1955.
2. K.J. Tauer and R.J. Weiss, *Bull. Amer. Phys. Soc.* **6**, 125, 1961.
3. L. Kaufman, E.V. Clougherty and R.J. Weiss, *Acta Metall.* **11**, 323–335.
4. S.C. Abrahams, L. Guttman and J.S. Kasper, *Phys. Rev.* **127**, 2052, 1962.
5. C. Kimball, W.D. Gerber and A. Arrott, *Bull. Amer. Phys. Soc.* **7**, 278, 1962.
6. U. Gonser, C.J. Meedian, A.H. Muir and H.J. Wiedersich, *J. Appl. Phys.* **34**, 2373, 1963.
7. F. Fitzgerald, *Metals and Materials*, **7**, 378–387, 1991.
8. R.F. Decker and S. Floreen: *Reference unknown*, 1986.
9. E. Hornbogen, *Innovations in Ultrahigh Strength Steel Technology*, 34th Sagamore Army Materials Research Conference, New York, 119–126, 1987.
10. S.S. Brenner, *J. Appl. Phys.* **27**, 1484–1491, 1956.
11. J.F. Knott, *Atomisitics of Fracture*, (eds R. M. Latanision and J.R. Pickens), 209–240, Plenum Publishing Corporation, UK, 1983.

12. *Encyclopaedia Brittanica*, **10**, 480, 1950.
13. E.A. Shipley, *High Strength Steels*, Special Report No. 76, 93, Iron and Steel Institute, 1962.
14. T. Inoue (Kobe Steel), *Private communication* to H.K.D.H. Bhadeshia, 1991.
15. E. Houdremont and H. Schrader, *Archiv für Eisenhüettenwesen*, **7**, 523–534, 1932.
16. E.S. Davenport, *Transactions of the American Society for Metals*, **27**, 837, 1939.
17. Anonymous, *Kobelco Technology Review No. 8*, Kobe Steel, Ltd., Japan, June 1990.
18. J.P. Naylor, *Spring Conference on Grain Boundaries*, Institution of Metallurgists, Series 3, No. 5, London, F13–17, 1976.
19. J.P. Naylor, *Metall. Trans. A* **10**, 861–873, 1979.
20. D.G. Brandon, B. Ralph, S. Ranganathan and M.S. Wald, *Acta Metall.* **12**, 813–821, 1964.
21. G. Langford and M. Cohen, *Trans. ASM*, **62**, 623, 1969.
22. G. Langford and M. Cohen, *Metall. Trans.* **1**, 1478–1480, 1970.
23. T.L. Altshuler and J.W. Christian, *Proc. Roy. Soc., London*, **A261**, 253–287, 1967.
24. W.C. Leslie, *Metall. Trans.* **3**, 5–26, 1972.
25. G.R. Speich and H. Warlimont, *J. ISI*, **206**, 385–392.
26. H.K.D.H. Bhadeshia, Unpublished research, 1991.
27. S.B. Newcomb and W.M. Stobbs, *Mater. Sci. Eng.*, **66**, 195–204, 1984.
28. D. Kalish and M. Cohen, *Mater. Sci. Eng.*, **6**, 156–166, 1970.
29. H.K.D.H. Bhadeshia, *Acta Metall.* **28**, 1103–1114, 1980.
30. J.S. Benjamin, *Metall. Trans.* **1**, 2943, 1970.
31. J.C. Baker and J.W. Cahn, *Solidification*, 23–58, ASM, Metals Park, Ohio, USA, 1971.
32. J.C. Baker and J.W. Cahn, *Acta Metall.* **17**, 575–578, 1969.
33. H.K.D.H. Bhadeshia, *Progress in Materials Science*, **29**, 321–386, 1985.
34. D.R. Maurice and T.H. Courtney, *Metall. Trans. A*, **21A**, 289–303, 1990.
35. M. Baloch, *Ph.D. Thesis*, University of Cambridge, 1988.
36. G.A.J. Hack, *Powder Metallurgy*, **27**, 73–79, 1984.
37. C.J. McMahon, Jr, *Innovations in Ultrahigh Strength Steel Technology*, 597–618, 34th Sagamore Army Materials Research Conference, New York, 1987.
38. S. Prakash, *Physical Review B*, **18**, 3980–3987, 1978.
39. L.B. Pfeil, *Proc. Roy. Soc.* **112**, 182–195, 1926.
40. A.R. Troiano, *Trans. ASM*, **52**, 54–80, 1960.
41. R.A. Oriani and P.H. Josefphic, *Acta Metall.*, **23**, 1065–1074, 1974.
42. F. Solana, C. Takamadate, I.M. Bernstein and A.W. Thompson, *Metall. Trans. A*, **18A**, 1023–1028, 1987.
43. S.K. Banerji, C.J. McMahon, Jr and H.C. Feng, *Metallurgical Transactions A*, **9A**, 237, 1978.
44. J.F. Watton, G.B. Olson and M. Cohen, *Innovations in Ultrahigh Strength Steel Technology*, 705–737, 34th Sagamore Army Materials Research Conference, New York, 1987.
45. G.B. Olson, *Journal of Materials Education*, **11**, 515–528, 1989.

46. G.B. Olson, J.F. Watton and M. Cohen, US Patent 4836869, referred to in: *J. Mater. Education*, **11**, 515–528, 1989.
47. H.K.D.H. Bhadeshia and J.W. Christian, *Metall. Trans. A*, **21A**, 767–797, 1990.
48. M. Takahashi and H.K.D.H. Bhadeshia, *Mater. Sci. Technol.*, **6**, 592–603, 1990.
49. E.S. Davenport and E.C. Bain, *Trans. TMS–AIME*, **90**, 117–154, 1930.
50. E.C. Bain, *Alloying Elements in Steel*, ASM, Cleveland, OH, USA, 1939.
51. K.J. Irvine and F.B. Pickering, *J. Iron Steel Inst.*, **188**, 101, 1958.
52. K.J. Irvine and F.B. Pickering, *ISI Special Report 93*, 110–125, Iron and Steel Institute, London, 1965.
53. H.K.D.H. Bhadeshia, *Steel Technology International, 289–294*, Sterling Publications, London, 1989.
54. H.K.D.H. Bhadeshia and A.R. Waugh, *Acta Metall.*, **30**, 775–784, 1982.
55. H.K.D.H. Bhadeshia and D.V. Edmonds, *Met. Sci.* **17**, 411–419, 1983.
56. H.K.D.H. Bhadeshia and D.V. Edmonds, *Met. Sci.* **17**, 420–425, 1983.
57. V.T.T. Miihkinen and D.V. Edmonds: *Mater. Sci. Technol.* **3**, 441–449, 1987.
58. J. Kalousek, D.M. Fegredo and E.E. Laufer, *Wear of Materials*, ed. K.C. Ludema, ASME, New York, USA, 212–231, 1985.
59. J. Kalousek and G. Beynon, *Rail Metallurgy*, Canadian Pacific Technical Reports, No. S497–75, 1975.
60. Collaborative research project between the University of Cambridge (H.K.D.H. Bhadeshia) and the British Steel Corporation (V. Jerath, K. Mistry, P. Bird and R.R. Preston), *British Steel Report SL/RS/R/S/1975/1/91A*, 1–43, 1991.
61. E.R. Parker, *Metall. Trans. A*, **8A**, 1025–1042. 1977.
62. R.O. Ritchie, M.H. Castro, V.F. Zackay and E.R. Parker, *Metall. Trans. A*, **9A**, 35–40, 1978.
63. J.H. Shively, R.F. Hehemann and A.R. Troiano, *Corrosion*, **22**, 253–256, 1966.
64. C.W. Marschall, R.F. Hehemann and A.R. Troiano, *Trans. ASM*, **55**, 135, 1962.
65. R.O. Ritchie, *Metal Science*, **11**, 368–381, 1977.
66. R. Kerr, F. Solano, I.M. Bernstein and A.W. Thompson, *Metall. Trans. A*, **18A**, 1011–1022, 1987.
67. Y. Tomita and K. Okabayashi, *Metall. Trans. A*, **14A**, 485–492, 1983.
68. Y. Tomita and K. Okabayashi, *Metall. Trans. A*, **14A**, 2387–2393, 1983.
69. Y. Tomita and K. Okabayashi, *Metall. Trans. A*, **16A**, 73–82, 1985.
70. Y. Tomita and K. Okabayashi, *Metall. Trans. A*, **16A**, 83–91, 1985.
71. Y. Tomita, *Metall. Trans. A*, **18A**, 1495–1501, 1987.
72. Y. Tomita, *Metall. Trans. A*, **19A**, 2513–2521, 1987.
73. T.A. Mutiu, A.J. Kinderman and I.M. Bernstein, *The Hot Deformation of Austenite*, (ed. J.B. Ballance), 410–427, TMS–AIME, New York, USA, 1977.
74. A. Ali and H.K.D.H. Bhadeshia, *Mater. Sci. Technol.* in press, 1991.
75. J.R. Patel and M. Cohen, *Acta Metall.*, **1**, 531–538, 1953.
76. J.W. Christian, *Metall. Trans. A*, **13A**, 509–538, 1982.
77. H.K.D.H. Bhadeshia, *J. of Mater. Sci.*, **17**, 383–386, 1982.
78. H.K.D.H. Bhadeshia, S.A. David, J.M. Vitek and R.W. Reed, *Mater. Sci. Technol.* in press, 1991.

79. A.A.B. Sugden and H.K.D.H. Bhadeshia, *Recent Trends in Welding Science and Technology*, (eds. S.A. David and J.M. Vitek), 745–748, ASM International, OH, USA (1989).
80. L.-E. Svensson and H.K.D.H. Bhadeshia, *Weld Quality and The Role of Computers*, 71–78, Pergamon Press, Oxford, 1988.
81. R.C. Reed, *Ph.D. thesis*, University of Cambridge, 1990.
82. R.C. Reed and H.K.D.H. Bhadeshia, *Recent Trends in Welding Science and Technology*, (eds S.A. David and J.M. Vitek), 205–210, ASM International, OH, USA, 1989.
83. G. Rees and H.K.D.H. Bhadeshia, *Unpublished research*, University of Cambridge, 1991.